ISSN 0016-7029, Geochemistry International, 2007, Vol. 45, No. 9, pp. 857–881. © Pleiades Publishing, Ltd., 2007.
Original Russian Text © O.A. Lukanin, A.A. Kadik, 2007, published in Geokhimiya, 2007, No. 9, pp. 933–961.

Decompression Mechanism of Ferric Iron Reduction in Tektite Melts during Their Formation in the Impact Process

O. A. Lukanin and A. A. Kadik

Vernadsky Institute of Geochemistry and Analytical Chemistry, Russian Academy of Sciences, ul. Kosygina 19, Moscow, 119991 Russia

e-mail: lukanin@geokhi.ru

Received March 1, 2006

Abstract—The analysis of available data on the Fe^{3+}/Fe^{2+} ratio of impact-produced glasses showed that tektites and some other types of impact glasses are reduced compared with the precursor target material. Possible reasons for the change in the degree of iron oxidation in the impact process are still debatable. Based on the analysis of redox reactions in relatively simple systems with iron in different oxidation states (Fe–O and SiO_2–FeO–Fe_2O_3) and the available data on the influence of temperature, oxygen partial pressure (pO_2), and total pressure (P_{tot}) on the Fe^{3+}/Fe^{2+} ratio of silicate melts, a model was proposed suggesting that the lower Fe^{3+}/Fe^{2+} values of tektites formed in the impact process compared with the initial target material could be related to the characteristics of oxygen regime during the decompression stage following shock compression. One of the main prerequisites for the occurrence of reduction reactions involving iron and other elements is the attainment of high temperatures (>1800–2000°C) at a certain stage of decompression, providing the complete melting and partial evaporation of the material. When the vapor pressure in the system becomes equal to the total pressure during adiabatic decompression, a further decrease in P_{tot} will be inevitably accompanied by a decrease in pO_2 and, correspondingly, partial reduction of Fe^{3+} to Fe^{2+} in the melt. The reactions of decompression reduction occur under closed-system conditions and do not require oxygen removal from the system. The higher the temperature and Fe^{3+}/Fe^{2+} ratio of the melt, the more extensive iron reduction can be observed during the final stages of decompression. If the temperatures attained during decompression after an impact event are sufficient (>2500–3000°C) for the complete evaporation of the material, the melt produced during subsequent condensation must be significantly more reduced than the initial material. The final stage of the impact process is characterized by a catastrophic expansion of the explosion cloud, condensation, and rapid cooling. During this stage, the system is already not closed. The quenched glasses of this stage record the redox state of earlier melts. In addition, they can contain microinclusions of the products of nonequilibrium vapor condensation with iron compounds of different oxidation states, including metallic iron and iron oxides (wüstite, magnetite, and hematite).

DOI: 10.1134/S0016702907090029

INTRODUCTION

Much of the interest in the investigation of impact phenomena, whose traces are preserved in the Earth's crust, stems from the fact that they may serve as a natural model for the processes that occurred during the early stages of Earth formation, when intense meteorite bombardment was among the main factors of planetary differentiation. The investigation of impact products and their experimental reproduction under laboratory conditions by applying ultrahigh pressures and temperatures to materials suggest that target rocks may experience significant chemical transformations during major impact events [1–4]. One remarkable chemical consequence of impact processes is the possibility of the occurrence of redox reactions involving changes in the oxidation state of iron and other elements. Such reactions are evidently responsible for the reduced character of tektite glasses, which are considered by most researchers to be produced by impact events on the Earth's surface during the last ~35 Myr of geologic history [3, 5–7, etc.]. Tektites show extremely low Fe^{3+}/Fe^{2+} values, much lower than those of felsic volcanic rocks of similar compositions and other terrestrial rocks that could serve as target sources during impact events.

Particular reasons for the impact-related changes in the degree of iron oxidation remain debatable [3, 6, 8–10]. Various mechanisms of Fe^{3+} reduction were proposed. (1) Processes of impact melt vaporization. Oxygen can be removed with a vapor phase during the melting and vaporization of the aluminosilicate material of a target under the high-temperature conditions (>2000°C) that are reached during impact events and characterize tektite formation. (2) Degassing of impact (tektite) melts with the release of gases of the C–O–H system. (3) Influence of the reduced material of an impactor (metallic iron and carbonaceous material) on the redox state of impactites produced by mixing the target and impactor materials. (4) Melting is accompanied by

reduction reactions owing to the presence of internal reducers in the initial target material, such as carbon (graphite), sulfur, and their compounds (hydrocarbons and sulfides). (5) Some researchers argued that tektite melts were formed by the condensation of a high-temperature vapor formed in the impact process. In their opinion, one possible reason for the reduced character of tektites is the fractionation of iron ions during the condensation of the vapor phase, i.e., preferential capture of Fe^{2+} by the melt compared with Fe^{3+} under the conditions of very rapid cooling.

This paper develops our concept that the main reason for the reduced state of tektite and some other impact-related glasses is reduction reactions involving iron and other element ions, which are controlled by regular changes in oxygen regime during the melting and evaporation of materials affected by an intense impact. Such reactions must inevitably occur during decompression under extremely high temperatures independent of the degree of system opening [10–12]. Therefore, the mechanism of ferric iron reduction in tektites considered here is probably more universal than the other mechanisms mentioned above. Before analyzing possible impact-related redox reactions involving iron ions, consider briefly the available data on the degree of oxidation and speciation of iron in impact glasses.

VALENCE STATE OF IRON IN TEKTITE AND IMPACTITE GLASSES

$Fe^{3+}/\Sigma Fe$ in Tektites

Tektites are natural glass bodies varying from a few millimeters (microtektites) to a few centimeters in size and having shapes suggesting, to a varying extent, aerodynamic ablation. They occur in extended strewn fields in various world regions. The very low contents of Fe^{3+} and water in tektite glasses compared with the rocks of the Earth's crust served as a basis for the suggestion on the origin of tektites by the impact melting of strongly reduced and extremely dry lunar rocks [13–15]. However, the geochemical evidence that has been accumulated up to now suggests that at least the main varieties of tektites were formed under terrestrial conditions owing to large impact events [1–3, 5–7]. Some tektite types were correlated with the formation of particular meteorite craters on the Earth's surface, which reliably constrained the compositions of the rocks that served as precursor materials for these tektites. This can be exemplified by moldavites, tektites from Central Europe, which were probably related to the impact event responsible for the formation of the Ries crater in southern Germany [6], and Ivory Coast tektites (western Africa), which were genetically connected with the Bosumtwi impact crater [7]. However, in contrast to glass-bearing impact rocks, parental impact craters and, correspondingly, target rocks are not reliably known for the majority of tektites.

One remarkable feature of the chemistry of tektite glasses is that their $Fe^{3+}/\Sigma Fe$ ratio is significantly lower than that of the target rocks that supposedly served as their precursors. Figures 1 and 2 summarize the available data on the degree of iron oxidation in the glasses of tektites and impactites as well as in the crustal rocks that potentially could serve as targets during impact events. The $Fe^{3+}/\Sigma Fe$ values determined by the most accurate chemical methods and Mössbauer spectroscopy range within 0.02–0.12 in tektites and >0.20–0.25 in the target rocks of various compositions and impact glasses found in or near impact craters.[1] The average $Fe^{3+}/\Sigma Fe$ values of felsic volcanic rocks that are chemically most similar to tektites are 0.25–0.50 (Fig. 2).

In general, tektites from different strewn fields (North America, Australia–Asia region, Central Europe, and West Africa) show no significant differences with respect to the degree of iron oxidation. There are probably some differences between the splash-form tektites and Muong Nong-type tektites, which have a layered texture and often show no distinct evidence for aerodynamic ablation on their surface. The Muong Nong-type tektites are chemically more heterogeneous and more often contain glasses with relatively high Fe^{3+} concentrations [19, 25]. The heterogeneity in the degree of iron oxidation may be observed within a single sample [20]. It should be noted that the unusually high values of $Fe^{3+}/\Sigma Fe > 0.35$ that were reported from Muong Nong-type indochinites by Koeberl et al. [25] were probably significantly overestimated, which is suggested by the results of subsequent investigations of tektites of this type using more sophisticated analytical methods. Moreover, a comparison of splash-form and Muong Nong-type tektites [8, 25] did not reveal any significant differences in terms of the iron oxidation state. Muong Nong-type tektites are widespread among indochinites and less common among other Australasian tektites. They are very rare in North America and Europe. It is supposed that Muong Nong-type tektites must occur closer to the parental impact craters compared with splash-form tektites, which may be dispersed by hundreds and even thousands of kilometers from the crater [5, 7].

No statistically significant difference in the degree of iron oxidation was ever detected within particular regional groups of splash-form tektites occurring within a single strewn field. This can be exemplified by the moldavites of Central Europa occurring in two

[1] $Fe^{3+}/\Sigma Fe$ was determined in tektite and impact glasses by various methods of wet and instrumental chemistry and by Mössbauer spectroscopy (MS). As the typical Fe^{3+} contents of tektites are low, some chemical methods overestimate their $Fe^{3+}/\Sigma Fe$ ratios compared with MS [8, 26]. The analysis of the obtained data supported the existence of real, although minor, variations in the $Fe^{3+}/\Sigma Fe$ ratio of tektites, not related to the accuracy of the analytical methods.

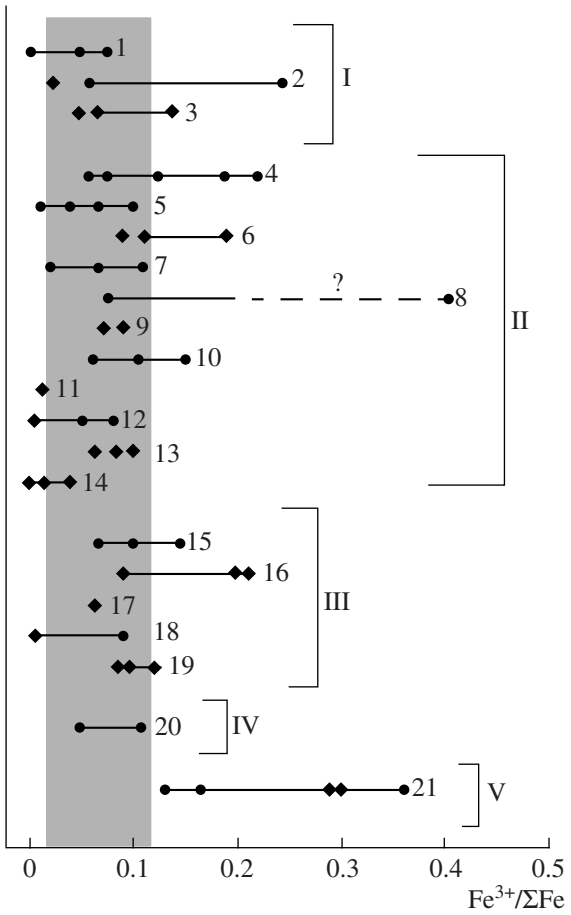

Fig. 1. Fraction of Fe^{3+} in the total iron content ($Fe^{3+}/\Sigma Fe$) of tektites and tektite-like glasses (irghizites) from various regions of the world. The analyses were obtained by wet chemistry (circles) and Mössbauer spectroscopy (diamonds). Mean and extreme values reported by various authors are shown in the diagram. (I) Tektites of North America: 1—bediasites, 21 samples [16]; 2—bediasites, six samples analyzed by wet chemical methods [17, 18] and one sample investigated by Mössbauer spectrometry [19]; and 3—georgiaites, three samples [20]. (II) Tektites from the Australasian strewn field: 4—australites, 31 samples [21, 22] and 34 samples from the Australasian region [18]; 5—australites and javanites, 12 samples [23] and average for four australite samples [14]; 6—three australite samples [24]; 7—philippinites and thailandites (Muong Nong type) [8]; 8—Muong-Nong-type tektites from the Australasian region, 18 samples [25]; 9—two indochinite samples [24]; 10—indochinites from Vietnam, 12 samples [15]; 11—philippinite-riasalite, one sample [19]; 12—two samples from Malaysia and two thailandite samples [26]; 13—three indochinite samples from Vietnam [27]; and 14—six indochinite samples [19]. (III) Tektites from Central Europe (moldavites): 15—22 samples [28]; 16—four samples [24]; 17—one sample [19]; 18—[26]; and 19—three samples [27]. (IV) Tektites from West Africa (Ivory Coast): 20—seven samples [29]. (V) Tektite-like glasses (irghizites) from the Zhamanshin crater, Kazakhstan: 21—three samples [30] and 20 samples [15] analyzed by wet chemistry and two samples investigated by Mössbauer spectroscopy [27].

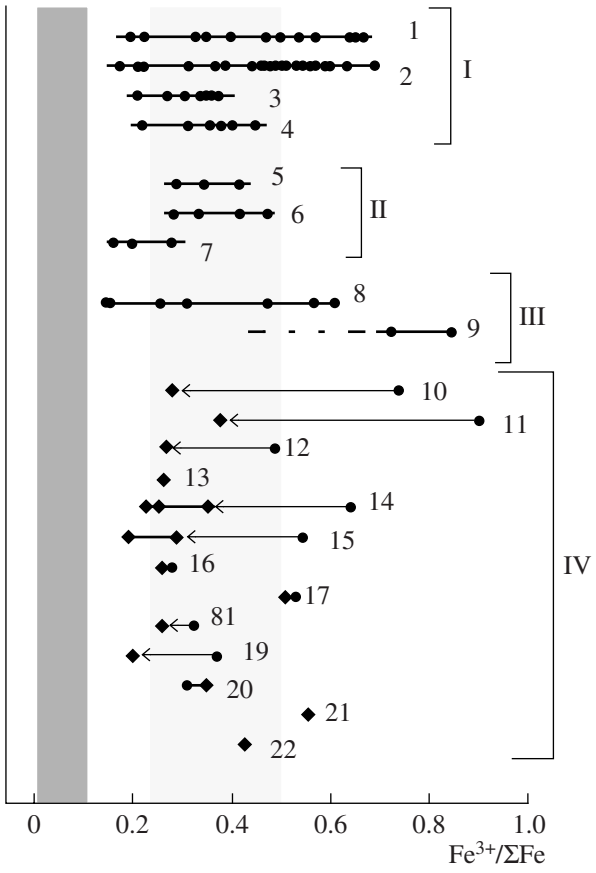

Fig. 2. Fraction of Fe^{3+} in the total iron content ($Fe^{3+}/\Sigma Fe$) of igneous, metamorphic, and sedimentary rocks of the Earth's crust and glasses of impactites and their initial target rocks from various impact craters. The rocks of the Earth's crust and the crustal rocks or their mixtures that supposedly served as precursors of impact melt rocks are indicated by circles, and the compositions of impact melt rocks are indicated by diamonds. (I) Igneous rocks: 1—granites; 2—felsic volcanic rocks (rhyolites, ignimbrites, and obsidians); 3—granodiorites and diorites; and 4—dacites and andesites [33]. (II) Metamorphic rocks: 5—felsic schists; 6—amphibolite-facies gneisses, and 7—granulite-facies gneisses and charnockites [34]. (III) Sedimentary rocks: 8—sandstones and graywackes and 9—shales [34]. (IV) Initial impactites and proposed precursor target rocks: 10—Wabar crater, Saudi Arabia [1]; 11—Aouelloul crater, western Sahara [1]; 12—New Quebec crater, Canada [35]; 13—Wanapitei structure, Canada [35]; 14—El'gygytgyn crater, Chukchi Peninsula, impact bombs, scoria, and pumices [1]; 15—Ries crater, Germany, impact bombs and impact melt rocks (suevites) [36]; 16—Janisjarvi crater, Russia [1]; 17—Kara crater, Russia [1]; 18—Popigai structure, Russia (Masaitis et al., 1976, cited after [1]); 19—Boltysh crater, Ukraine [1, 37]; 20—Charlevoix crater, Canada (Rondot, 1971, cited after [1]); 21—Manicougan crater, Canada [35]; and 22—Morokweng structure, South Africa [35]. The arrows indicate $Fe^{3+}/\Sigma Fe$ variations during the formation of impact melts (glasses) at the expense of initial target rocks.

regions of Bohemia and Moravia more than 100–150 km apart; the tektites of the Australasian region from Indochina, Indonesia, and Australia; and the bediasites and georgiaites of North America.

The reduced state of iron in tektite glasses was supported by the electrochemical measurements of intrinsic oxygen fugacity (fO_2) of tektite glasses at 500–1150°C, which appeared to be 1.5–2.0 logarithmic units lower than the fO_2 values of the magnetite–wüstite (MW) buffer and, correspondingly, much lower than the fO_2 values of the fayalite–magnetite–quartz (FMQ) buffer, which are characteristic of volcanic rocks near the Earth's surface [10, 31, 32].

$Fe^{3+}/\Sigma Fe$ of Impact Glasses

Glasses formed by rapid cooling of impact melts were described in various types of impactites, which occur near to or directly within meteorite craters. Among them are centimeter- and meter-sized impact bombs consisting of almost pure glass. Tektite-like impactites from the Zhamanshin impact crater in Kazakhstan (irghizites) can be assigned to the same type. Another variety is represented by massive impact melt rocks (tagamites) with widely varying glass contents occurring directly within impact craters.

Compared with tektites, the impact glasses show significantly higher $Fe^{3+}/\Sigma Fe$ values, mainly within 0.25–0.59 (IV in Fig. 2). Many authors have compared the chemical compositions of impact glasses with those of target rocks, which served as a source material for impact melts. The obtained data were summarized in a number of monographs and review papers. Some of them reported data on the redox state of iron in impactites and supposed precursor target rocks [1, 3, 35, 38], which allowed us to conclude that the formation of impact melts was often accompanied by the reactions of ferric iron reduction, resulting in a decrease in $Fe^{3+}/\Sigma Fe$ compared with the initial rocks [1, 3].

It should be noted that the problem of a change in the chemical composition and redox state of initial materials during impact events requires a sophisticated analysis of the composition of impactite and presumable target rocks. This is primarily important, because the sources of impact melts are usually mixtures of surface crustal rocks of sedimentary, metamorphic, and magmatic genesis. The model composition of target rocks is usually reconstructed as the most probable mixture of several components with different compositions and, correspondingly, different degrees of iron oxidation. The impactor material can also contribute to this mixture. In the case of an iron meteorite consisting of almost pure metallic iron, even a small admixture of the impactor material can significantly affect the oxidation state of iron in the impact melts, especially when the target rocks have very low contents of iron oxides.

The average contents of components, including FeO and Fe_2O_3, usually show rather large standard deviations both in impact glasses and target rocks. Therefore, conclusions drawn from a comparison of the compositions of impact glasses and target rocks should be considered in many cases as approximate tendencies in the transformation of initial materials, which require more detailed studies for their verification in particular complexes. The following general regularities (more precisely, tendencies) in relative changes in the redox state of iron during the formation of impact melts (glasses) can be deduced from the available data.

(1) Impact glasses formed mainly at the expense of strongly oxidized rocks (usually of sedimentary origin: sandstones, clayey rocks, etc.) in relatively small impact craters show a significant reduction of Fe^{3+} during their formation. This can be exemplified by impact glasses from the Henbury (5–160 m in diameter), Wabar (91 m in diameter), and Aouelloul (350 m in diameter) meteorite craters, which have $Fe^{3+}/\Sigma Fe$ values of 0.25–0.40 and were formed by the impact melting of sedimentary rocks, mainly sandstones, with $Fe^{3+}/\Sigma Fe > 0.7$. A possible reason for the reduced composition of some of these glasses is the contribution of the meteorite impactor material to their formation. Indeed, the presence of iron meteorite material in the dark-colored (black) varieties of impact glasses from these craters was supported by their geochemical signatures. It should also be noted that, in addition to black glasses, the Wabar and Aouelloul craters contain light colorless glasses, which are also reduced relative to the target rocks but show no evidence for a significant contamination with meteoritic iron [1, 3, 38] (16 and 17 in Fig. 2). Thus, the leading role of contamination with meteoritic material for the reduction of iron in these glasses is not evident, and other mechanisms can be proposed for Fe^{3+} reduction during their formation.

Contamination with meteoritic material of chondritic composition can be exemplified by glasses genetically related to the New Quebec (3.4 km in diameter) and Wanapitei (~8 km in diameter) impact craters in Canada. These glasses have rather low $Fe^{3+}/\Sigma Fe$ values of 0.25–0.27 (18 and 19 in Fig. 2), and it can, therefore, be supposed that their formation was accompanied by the partial reduction of Fe^{3+} from the targets, which were composed of granitoid gneisses and metasediments. An admixture of up to 2% chondritic material (C1-type for the glasses of the New Quebec crater) is supposed for both glass types [35]. It is not yet clear whether the presence of the impactor material is the main factor responsible for reduction during the formation of these impact melts.

Thus, it can be concluded that the aforementioned impact craters contain impact glasses of rather diverse compositions. Some of them were obviously significantly contaminated with meteoritic material. In the cases of a significant contribution from iron meteorite material, the resulting glasses show a notable increase in total iron content and a significant decrease in $Fe^{3+}/\Sigma Fe$. There is little doubt that the redox state of

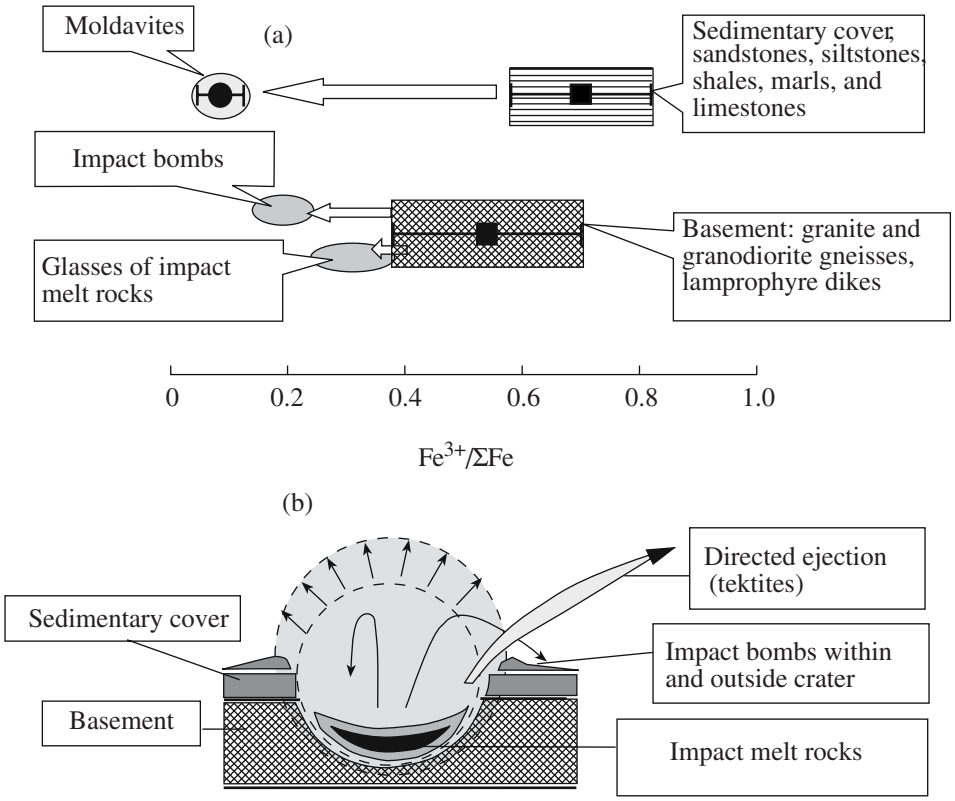

Fig. 3. (a) Relationships between the degrees of iron oxidation in target rocks and impact products by the example of the Ries impact crater. The majority of data are after Engelhardt et al. [39, 40] summarized in part by Dressler and Reimold [35]. (b) Cartoon illustrating the origin of various "facies" of impact rocks by the example of the Ries crater in southern Germany. Tektites are produced by the melting, evaporation, and condensation of materials mainly from the sedimentary cover. Impact bombs are formed mainly at the expense of basement rocks and occur both within and outside the impact crater. Impact melt rocks are partly molten basement rocks remaining within the crater after the impact. A mixture of partly molten rocks and impact bombs often occurs within natural craters.

iron in such impact glasses was affected by the impactor material. On the other hand, relatively reduced glasses not affected by any significant contamination with meteorite material may occur in the same craters. Other mechanisms can be supposed for the reduction of such glasses.

(2) In some relatively large impact craters, the effect of Fe^{3+} reduction during the formation of impact melts is established rather reliably by a comparison of the compositions of target rocks and glasses from impact bombs, which may occur both within and outside the impact craters. It should be emphasized that they usually do not show compelling evidence for a significant contamination with the impactor material. This can be exemplified by impact bombs from the El'gygytgyn crater in the Chukchi Peninsula (18 km in diameter), which show much lower $Fe^{3+}/\Sigma Fe$ values than the initial material, 0.23 and 0.64, respectively (14 in Fig. 2). A similar situation was observed in the Ries impact crater in southern Germany (24 km in diameter, Fig. 3a), where $Fe^{3+}/\Sigma Fe$ values of glasses from impact bombs occurring both within and outside the crater are significantly lower than in the precursor basement rocks (Fig. 3b).

It is evident that tektite-like irghizite glasses can also be assigned to this group. They occur near the Zhamanshin crater in Kazakhstan (13 km in diameter) and are usually similar in shape and size to volcanic lapili. Their $Fe^{3+}/\Sigma Fe$ value ranges within 0.15–0.30. This is much lower than the $Fe^{3+}/\Sigma Fe$ value of their supposed precursor rocks, which were dominated by loess-like sediments [3, 15] (V in Fig. 1). Note that the most reduced irghizite samples are similar in terms of $Fe^{3+}/\Sigma Fe$ values to Muong Nong-type tektites.

(3) The major portion of melt phase produced during the formation of large impact craters remains within the craters as impact melt rocks (tagamites). Their iron oxidation state is practically identical to that of the target rocks. This can be exemplified by tagamites from the Janisjarvi (Russia, 14 km in diameter), Kara (Russia, 65 km in diameter), Popigai (Russia, 100 km in diameter) [1], and Boltysh (Ukraine, 25 km in diameter) impact craters [1, 37]. The impact melt rocks of the Ries crater contain 40–50% glasses, which are much less reduced than the glasses of impact bombs. Within

the analytical error, their $Fe^{3+}/\Sigma Fe$ values are identical to those of the target rocks, which are dominated by granitic gneisses and minor amphibolites (Fig. 3). Impact melt rocks from the older giant impact craters of Morokweng (South Africa, 70–80 km in diameter) and Manicouagan (Quebec, Canada, 100 km in diameter) show relatively high $Fe^{3+}/\Sigma Fe$ values of 0.4–0.6 [35]. If these values correspond to the initial state of impact melts, it can be concluded with confidence that the target rocks were not significantly reduced during the impact event.

The following conclusions can be drawn from the short overview of the available data on the relations of various valence states of iron in tektite and impactite glasses. (1) The highest degree of reduction of target rocks during impact events is observed in tektite melts (glasses). (2) The formation of the major portion of impact melt rocks experiencing only minor displacements (tagamites) was accompanied by negligible changes in the degree of melt oxidation compared with the initial rocks. (3) In terms of the degree of reduction, the melts of impact bombs, including such tektite-like objects as irghizites, occupy an intermediate position between tektites and impact melt rocks. In general, the degree of impact melt (glass) reduction compared with their precursor target rocks increases in the following sequence: impact melt rocks (tagamites)–impact bombs–tektite-like impactites (irghizites)–Muong Nong tektites–splash-form tektites.

Various types of impact melts, which are represented by the glasses of tektites, impact bombs, and tagamites, were formed under different thermodynamic conditions, which allowed some researchers to interpret them as products of different facies of the impact process [3]. Temperature is obviously among the main factors controlling their chemical characteristics and structural state. Tektites are the highest temperature objects. According to various estimates, the temperatures of their formation were higher than 2000°C and could be as high as several thousand degrees [1–3]. Impact bombs were formed at much lower temperatures, probably no higher than 1800–2000°C. Tagamites are characterized by the lowest temperatures in this sequence. Complete melting was usually not attained in them, and their temperature was probably no higher than 1600–1800°C.

IRON SPECIATION IN TEKTITE AND IMPACTITE GLASSES: STRUCTURAL POSITION OF IRON IN GLASSES AND IRON-BEARING MICROINCLUSIONS

The previous section presented data obtained by the analysis of iron in natural tektite and impactite glasses, which were carefully picked to avoid sample contamination with foreign phases occurring in glasses. However, during the analysis by wet chemistry methods and Mössbauer spectroscopy, the presence of submicroscopic mineral phases in the samples cannot be fully ruled out. Moreover, it should be noted that iron-bearing phases were found as microinclusions in impact glasses and can be used as indicators of redox conditions during their formation. In this context, it is instructive to consider the available data on iron speciation in the glass structure and occurrence as microscopic and submicroscopic inclusions.

Structural State of Fe^{2+} and Fe^{3+}

According to the data of Mössbauer spectroscopy (MS), the average hyperfine interaction parameters of the most abundant iron ions (Fe^{2+}) in impact glasses are intermediate between the values characteristic of octahedral and tetrahedral oxygen polyhedra in iron-bearing mineral phases [19, 24, 26, 27, 41]. The coordination number of the major portion of Fe^{2+} in tektites is estimated as between 6 and 5 [19, 41] or close to 5 [26]. Some researchers used recent sophisticated methods for the processing of Mössbauer spectra and concluded that ferrous iron may occur in tektite glasses in both near octahedral (most abundant) and tetrahedral (about 10%) coordinations [19, 26]. The investigation of glasses by EXAFS and XANES showed that the average coordination number of Fe^{2+} in tektites can be between 4 and 5 [42]. Thus, in both types of impact glasses, the oxygen environment around Fe^{2+} probably approaches a significantly distorted octahedron. In general, the data of MS, EXAFS, and XANES investigations suggest that the degree of structural ordering if Fe^{2+} in glasses increases in the sequence tektite–impact bombs–impact melt rocks (tagamites) [24, 41, 42].

In impact bombs and tagamites as well as in tektite-like glasses (irghizites), Fe^{3+} occurs mainly in tetrahedral oxygen coordination [24, 41]. The Fe^{3+} content of tektite glasses is fairly low, and the MS data on its structural state are controversial. Depending on the applied methods of the description and interpretation of MS spectra, Fe^{3+} is assigned either to mainly tetrahedral [24] or octahedral coordination [41]. According to the data of Dunlap et al. [19], the structural position of Fe^{3+} cannot yet be determined by MS because of the low Fe^{3+} content. Moreover, Rossano et al. [26] even questioned the validity of MS for the determination of the fraction and structural state of Fe^{3+} in reduced tektite glasses, for instance, in moldavites. They suggested that Fe^{3+} is either completely lacking in them or its content is below the sensitivity limit of MS. On the other hand, the investigation of tektites by electron paramagnetic resonance (EPR) provided compelling evidence for the presence of ferric iron in the glass structure, although its quantitative analysis by this method is a difficult task [3, 8, 43]. The presence of the (Fe^{3+}–O_4) structural groups in the glasses of moldavites and indochinites was established by EPR spectroscopy [3]. Thus, there is no reason to doubt that some fraction of iron occurs as Fe^{3+} even in the structure of the most reduced tektite glasses.

Submicroscopic and Microscopic Iron-Bearing Inclusions

In addition to iron ions incorporated in the glass structure, the EPR method reveals submicroscopic or cryptocrystalline iron-bearing phases, whose sizes are estimated as about 100 Å. According to Mineeva et al. [44], such phases in tektite glasses (moldavites and indochinites) are represented by magnetite and hematite, and impact glasses from the El'gygytgyn crater contain also jacobsite ($MnFe_2O_4$) and probably other unidentified phases. Raikhlin et al. [43] investigated tektite and impactite glasses by EPR spectroscopy and concluded that ferric iron occurs in them both in the glass structure and "as Fe^{3+} associations in magnetic clusters" and submicroscopic magnetite grains. According to their results, both types of glass contained very small amounts (if any) of submicroscopic hematite inclusions. It was noted that the content of iron in magnetic clusters and/or submicroscopic magnetite inclusions in impact glasses and irghizites is much higher than in tektites.

Even a wider set of iron-bearing phases was revealed in impact glasses as microinclusions (accessory minerals) varying from several micrometers to hundreds of micrometers in size. In addition to magnetite and hematite, the impactite glasses contain titanomagnetite in association with ilmenite, armalcolite ($Fe_{0.5}Mg_{0.5}Ti_2O_5$), and iozite (FeO) replaced by magnetite [3, 45]. Of special interest are the findings of spherical metallic Fe–Ni microinclusions in impact glasses. They were described in glasses from many impact craters: Wabar, Bosumtwi, Ries, Aouelloul, Ilyinets, Boltysh, Kara, and Lappajarvi [3, 45–49]. Their metallic phase (kamacite) coexists with troilite, schreibersite, iozite, and cohenite. It is noteworthy that, in addition to the inclusions of metallic Fe–Ni phase in which Ni content is higher than several weight percent, spherules of native iron with low Ni content (<0.1–0.4 wt %) were found in impactite glasses. They contain tiny grains of wüstite, occasionally with cohenite inclusions (Zapadnyi, Ilyinets, Rotmistrovsky, Boltysh, and Kara craters, as well as the Janisjarvi and Gardnos craters of the Baltic shield) [3, 45, 50]. In such inclusions, metallic Fe makes up the cores of spherules and is mantled by more oxidized minerals, up to maghemite (oxymagnite). The inclusions of native iron in these glasses coexist with magnetite spherules with pores in the central part. It is interesting that similar metallic and iron oxide inclusions were found in volcanic rocks, where their formation was attributed to the activity of relatively reduced magmatic gases and fluids [51].

Spherical microinclusions of metallic iron with a nickel impurity, ~1–800 μm in diameter were found in some tektite glasses. They were first discovered in some samples of Philippine tektites and, then, in the indochinites of Vietnam [52, 53]. Most of the inclusions contain kamacite, schreibersite (Fe_3P), and troilite. Their external appearance, internal structure, and mineral composition are similar to those of Fe–Ni inclusions in impactites. However, a detailed examination of the composition of the metallic phase showed that its Ni content is significantly lower than in the similar inclusions from impactites. The concentration of Ni is 1–3 wt % for the Philippine tektites and 4–6 wt % for the Vietnam indochinites. For comparison, the contents of Ni in Fe–Ni inclusions in glasses is 9.6 wt % in the Aouelloul crater [48] and 8–14 wt % in the Wabar crater, reaching 32–40 wt % in some inclusions [54].

In contrast to impactites, inclusions of native iron with very low Ni contents were never detected in tektite glasses. Inclusions of native iron replaced by magnetite were documented in glasses from the Libyan Desert, but they are not typical tektites [13, 55]. On the other hand, several authors described magnetite microinclusions in tektite glasses [13, 56, 57].

The presence of submicroscopic inclusions of metallic iron in tektite glasses was supposed on the basis of the measurements of their magnetic properties. Thorpe and Senftle [58] measured the magnetic susceptibility of 18 samples of tektite glasses from various regions of North America, Central Europe, Thailand, Indochina, and the Philippines and concluded that the obtained data could be best interpreted by assuming the presence of submicroscopic (<1 μm) inclusions of metallic iron similar to larger metallic inclusions found in some samples of Philippine tektites. The same authors analyzed the available spectrophotometric data for tektite glasses and supposed that variations in tektite color from brown to black could be related to the presence of finely dispersed colloidal particles of hematite and/or metallic iron in glasses. On the other hand, an investigation of the magnetic susceptibility of a large group of tektites, including 166 samples of australites, indochinites (including Muong Nong-type tektites), and moldavites performed by Werner and Borradaile [59] showed that the ferromagnetic contribution is very small compared with the paramagnetic one, and, therefore, the content of ferromagnetic phases (magnetite, metallic iron, or metallic nickel) is negligible in all of the samples.

In summary, the above data allow us to make the following conclusions concerning the speciation of iron in impact glasses. (1) In tektite and impactite glasses, Fe^{2+} and Fe^{3+} occur both in certain positions in the glass structure and in cryptocrystalline phases and mineral microinclusions, which are much more common in impactite glasses than in tektites. (2) In addition to the mineral microinclusions of magnetite, hematite, wüstite (iozite), and other iron oxides (containing also Ti and Mn), many impactite glasses contain spherules of metallic iron with high (>8–9 wt %) and very low (<0.4 wt %) Ni abundances. (3) Magnetite microinclusions were found in tektite glasses. In addition, their EPR spectra and magnetic properties suggest the presence of submicroscopic hematite grains in them. (4) Up to now, metallic Fe–Ni microinclusions with

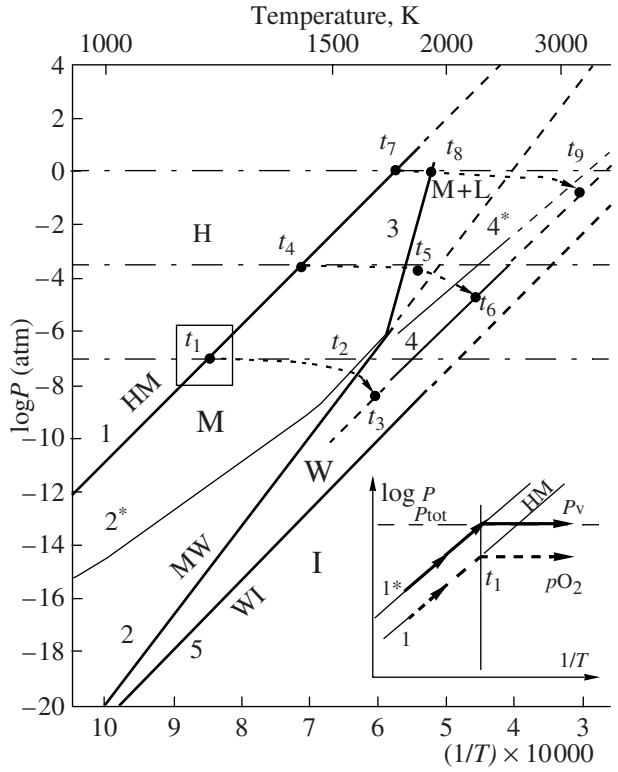

Fig. 4. Thermal reduction of ferric iron in the Fe–O system. The influence of temperature on oxygen partial pressure (pO_2) and total vapor pressure (P_v) for various phase assemblages in the iron–oxygen system [63, 64]. Phase abbreviations: I, iron; H, hematite; M, magnetite; and W, wüstite. Bold lines 1–5 indicate variations in oxygen partial pressure for various phase assemblages: 1, hematite–magnetite (HM); 2, magnetite–wüstite (MW); 3, magnetite–iron oxide melt (ML); 4, congruent transformation of wüstite from a condensed (crystalline or liquid) to a gaseous state; and 5, wüstite–iron (WI). The thin lines marked by numbers with asterisks show P_v variations for the same equilibria: 1*, HM; 2*, MW; and 4*, congruent melting and evaporation of wüstite. Line 1* is shown in the inset only, because it almost coincides with line 1 on the scale of the diagram, which is related to the fact that the vapor phase consists of almost pure O_2, i.e., $P_{tot} \approx pO_2$. Variations in P_v for the IW assemblage are not shown to avoid overcrowding. The arrow-headed dashed lines show pO_2 variations with increasing temperature at a constant total pressure (P_{tot}). Three cases are shown for the heating of the initial hematite–magnetite mixture at P_{tot} of 10^{-7}, $10^{-3.5}$, and 1 atm. The inset in the lower right illustrates the position of P_v and pO_2 trends during the heating of the hematite–magnetite mixture approximately at temperature t_1 and $P_{tot} = 10^{-7}$ atm. The solid line with arrows shows P_v variations, and the dashed line with arrows is the trend of pO_2. When temperature t_1 is reached, the vapor pressure for the hematite–magnetite mixture becomes equal to the total pressure, $P_v = P_{tot} = 10^{-7}$ atm. Further temperature increase at $P_v = P_{tot} = \text{const}$ is accompanied by a minor decrease in pO_2 in the system. See text for further explanation.

<4–6 wt % Ni, which is much lower than the Ni content of the Fe–Ni inclusions of impactites, have been found only in rare samples of Australasian tektites. Inclusions of Ni-free metallic iron were never detected in tektite glasses. The magnetic properties of tektite glasses indicate the possible presence of very small amounts of colloidal size particles of native iron. It is not yet clear whether such a phase exists and, if it does, how much Ni it contains.

It is important to emphasize that the glasses of impact origin contain microscopic and submicroscopic inclusions of iron-bearing mineral phases, some of which obviously cannot be in equilibrium with each other. The coexistence of metallic iron (and/or wüstite) with hematite and magnetite may serve as an example. Such associations probably owe their existence to nonequilibrium processes during various stages of tektite and impactite formation: protolith melting, condensation, cooling, and complete solidification of impact melts. The Ni-rich metallic inclusions coexisting with schreibersite and troilite are evidently related to a meteorite source [53, 54]. However, the mechanisms of their formation and the influence of such inclusions on the redox state of the host glasses are not fully understood. The metallic inclusions with negligible or minor Ni contents could probably be related to a different, nonmeteoritic source. It was supposed that the presence of reducers in the initial materials (for instance, carbon and its compounds) could be responsible for the formation of such inclusions. On the other hand, they could be produced by the nonequilibrium condensation of an impact-generated vapor phase, which contains zero-valence iron and other metals.

REDUCTION OF FERRIC IRON IN OXIDE SYSTEMS IN RESPONSE TO CHANGES IN *P–T* CONDITIONS

Before discussing the possible reduction mechanisms of tektites and impactites, which usually have complex multicomponent compositions, we consider some important features of redox reactions accompanying changes in *P–T* parameters in relatively simple systems containing iron in different oxidation states: Fe–O and SiO_2–FeO–Fe_2O_3.

Fe–O System

Let us begin with the simplest Fe–O system, which is rather well studied both experimentally and theoretically [60–65]. Figure 4 shows variations with temperature in total vapor pressure (P_v) and oxygen partial pressure (pO_2) in equilibrium with phases containing iron in different oxidation states.[2] At a constant total pressure (P_{tot}), initial compositions containing mainly ferric iron must be reduced at increasing temperature in

[2] $P_v = \Sigma p_i$, where p_i is the partial pressure of component i in the vapor phase. The main components of the vapor phase in the Fe–O system are O_2, O, Fe, and FeO. If total pressure in the system (P_{tot}) is imposed by an inert gas, then P_v equals the sum of the partial pressures of all components of the Fe–O system in the gas phase and $P_{tot} > P_v$. If P_{tot} is imposed by an inert condensed phase and $P_{tot} > P_v$, there is no vapor (gas) phase in the system.

both closed and open systems, when the gas phase produced by reduction is removed from the system. This process of thermal reduction (or thermal dissociation according to a more general nomenclature by Kulikov [63, 64]) can be observed in more detail in Fig. 5. This diagram presents isobaric sections of the Fe–O system, which were constructed by us on the basis of the thermodynamic analysis of phase equilibria in this system [64] and, in particular, calculations of partial pressures for the main components of the vapor phase.

For initial composition **a** consisting of a hematite (H)–magnetite (M) mixture with the prevalence of the former at $P_{tot} = 10^{-7}$ atm (Fig. 5a), P_v and pO_2 increase with increasing temperature (>1000°C). The condition $P_v = P_{tot}$ is reached at t_1. Since the vapor phase in equilibrium with the hematite–magnetite assemblage is composed of almost pure molecular oxygen at this temperature, the pO_2 value of the system approaches P_{tot} (inset in Fig, 4). Upon further heating, temperature increases only after the complete decomposition (dissociation) of hematite with the formation of the magnetite solid solution. As a result, the Fe^{3+}/Fe^{2+} ratio of the condensed phase decreases dramatically. As temperature increases above t_1, the composition of the magnetite solid solution (Mss) changes to lower Fe^{3+}/Fe^{2+} values. The fraction of iron atoms in the vapor phase increases, iron partial pressure (pFe) increases, and pO_2 decreases accordingly. The composition of the vapor is enriched in iron, and its Fe/O ratio increases. At a temperature of t_2, magnetite becomes unstable and is reduced to the wüstite solid solution. An increase in temperature is accompanied by an abrupt decrease in the Fe/O and Fe^{3+}/Fe^{2+} values of the condensed phase. A further temperature increase is accompanied by a gradual reduction of the wüstite solid solution and a considerable increase in pFe. The degree of the thermal reduction of the condensed phase depends on whether the system is closed or not. In a closed system, the initial material is completely vaporized at a temperature corresponding to point V_a (Fig. 5a). The maximum reduction that can be reached in the condensed phase corresponds to the wüstite composition W_a. Under open-system conditions, when the gas phase is removed from the system, the degree of condensed phase reduction can be somewhat higher. In such a case, the resulting Fe^{3+}/Fe^{2+} values can correspond to the composition of wüstite (W_m) which evaporates congruently at t_3. Thus, all the initial compositions of the system with oxygen contents higher than that in point W_m undergo thermal dissociation and reduction at isobaric heating. However, the most reduced composition of the condensed phase cannot contain less oxygen and, correspondingly, Fe^{3+} than the composition of W_m.

A temperature increase under isobaric conditions at higher P_{tot} values also leads to the reduction of composition **a** and other oxidized initial compositions (Figs. 5b, 5c). As P_{tot} increases, the temperatures of hematite and magnetite decomposition corresponding to abrupt decreases in the Fe^{3+}/Fe^{2+} ratio of the condensed phase increase. In contrast to the case with $P_{tot} = 10^{-7}$ atm, the decomposition of magnetite at $P_{tot} = 10^{-3.5}$ and $P_{tot} = 1$ atm is accompanied by the formation of oxide melt, L_{ox}, rather than wüstite. The composition of L_{ox} becomes progressively more reduced with increasing temperature. The extreme Fe^{3+}/Fe^{2+} ratio of this melt corresponds to the composition of L_m, which evaporates congruently similar to the W_m wüstite composition. The compositions W_m and L_m become enriched in iron with increasing P_{tot}, approaching the stoichiometric FeO composition.

It should be noted that the existence of a temperature maximum on the vapor line at W_m and L_m provides a possibility for the thermal oxidation of iron-rich initial compositions lying on the composition axis left of the maximum points (Figs. 5a–5c). Indeed, during the heating of the iron–wüstite mixture (I + W), atomic iron is the main component of the vapor phase, and the stability temperature of the metal phase (solid or liquid) is therefore lower than that of the oxide phase. As a result, the metallic phase disappears first during a temperature increase, and the residual oxide phase is enriched in oxygen and, correspondingly, Fe^{3+}.

It is important for the solution of the problem of reasons for the reduction of tektite and impactite glasses that a temperature increase under isobaric conditions is not the only way to change the degree of iron oxidation. A characteristic feature of the Fe–O and other systems containing iron in different oxidation states is the possibility of redox reactions induced by a decrease in the total pressure of the system. This is especially important for the analysis of the behavior of materials in impact processes, because the melting and vaporization of materials affected by an impact event take place in such a case during the stage of unloading under near adiabatic decompression conditions.

Figure 6 presents a section of the Fe–O system at a temperature of 1870°C constructed using the data of [64], which illustrates a change in the oxidation state of Fe in oxide melts affected by isothermal decompression. As can be seen from the phase diagram shown in Fig. 6, initial composition **a**, which contains mainly ferric iron and corresponds to hematite in Fe/O ratio, produces an oxygen-dominated vapor phase when pressure decreases below $P_1 \sim 10$ atm. As pressure further decreases, the composition of the condensed phase changes along the line of liquid toward the L_m point, corresponding to the composition of liquid congruently evaporating under this temperature. The oxide melt is enriched in iron and becomes more reduced toward L_m, and the fraction of atomic Fe in the equilibrium vapor increases (Fig. 7). Under closed-system conditions, the melt evaporates completely at P_2 ($\sim 10^{-5.2}$ atm). The composition of vapor corresponds under this pressure to the initial composition of the oxide melt, and the last portion of melt has a wüstite composition, L_{ox}, very similar to L_m (Fig. 6). Under open-system conditions when the released gas phase is removed instantly from

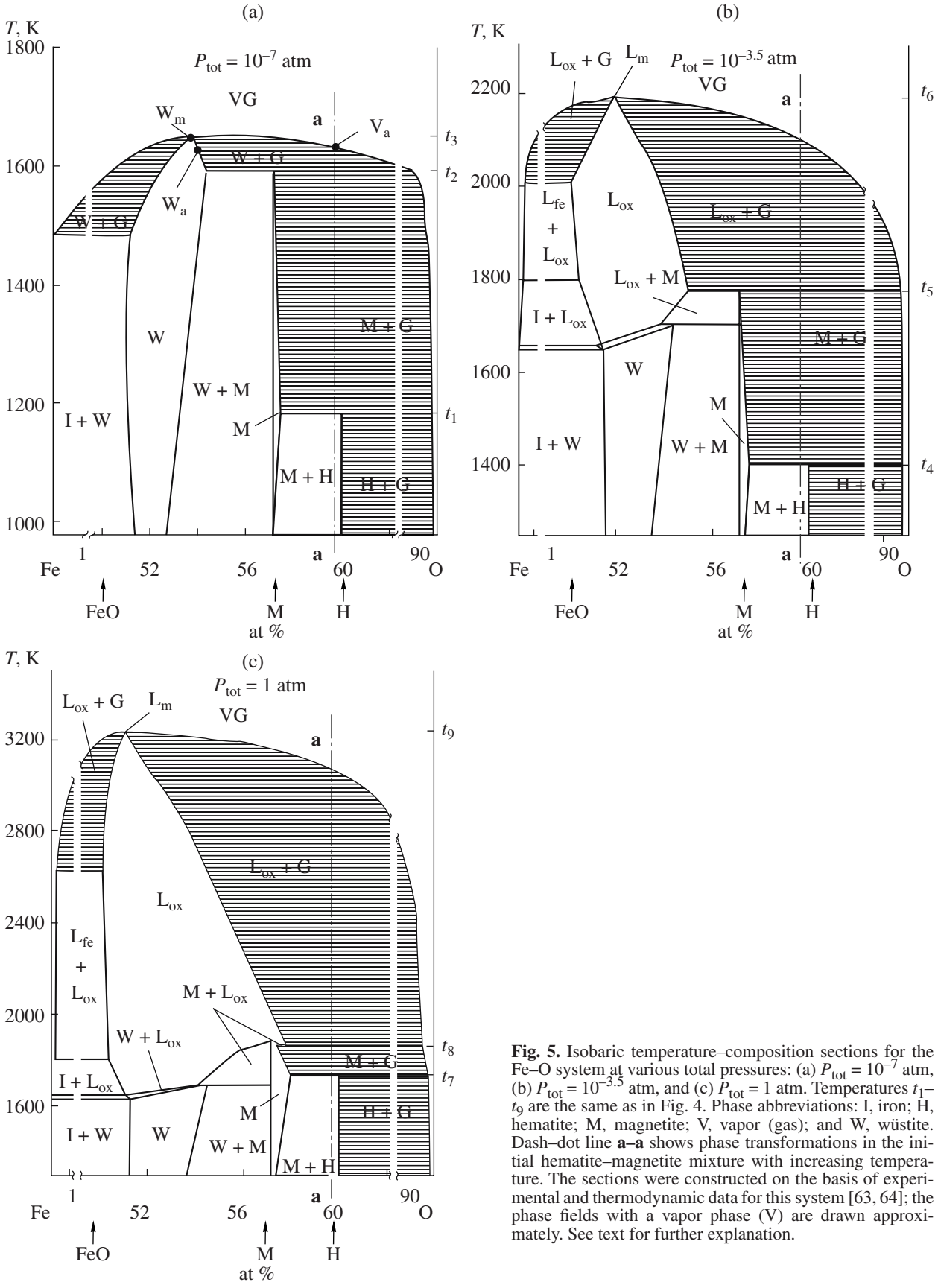

Fig. 5. Isobaric temperature–composition sections for the Fe–O system at various total pressures: (a) $P_{tot} = 10^{-7}$ atm, (b) $P_{tot} = 10^{-3.5}$ atm, and (c) $P_{tot} = 1$ atm. Temperatures t_1–t_9 are the same as in Fig. 4. Phase abbreviations: I, iron; H, hematite; M, magnetite; V, vapor (gas); and W, wüstite. Dash–dot line **a–a** shows phase transformations in the initial hematite–magnetite mixture with increasing temperature. The sections were constructed on the basis of experimental and thermodynamic data for this system [63, 64]; the phase fields with a vapor phase (V) are drawn approximately. See text for further explanation.

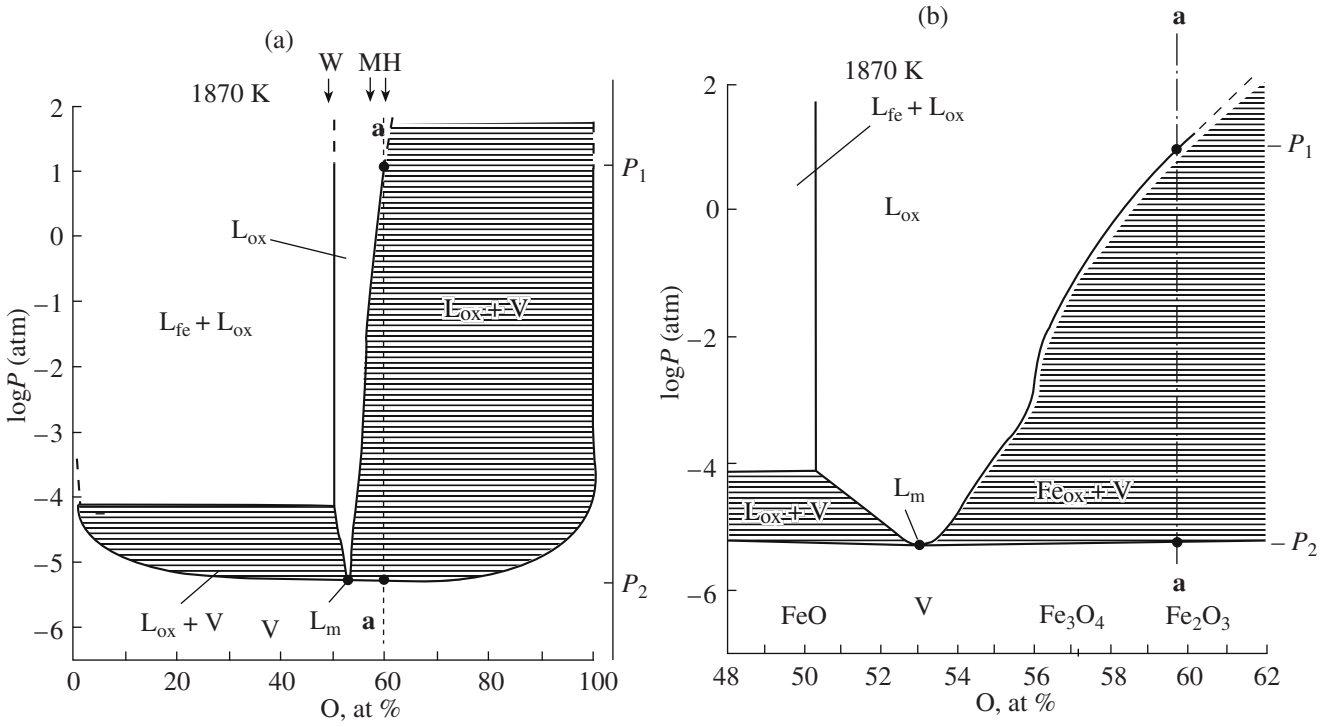

Fig. 6. Decompression reduction of iron oxides in the Fe–O system. (a) Isothermal section of the Fe–O system at 1870 K constructed on the basis of data of [64]. (b) An enlarged fragment of the same isothermal section. Phase abbreviations: L_{fe}, metallic iron melt; L_{ox}, iron oxide melt; and L_m, the composition of iron oxide melt congruently evaporating at decreasing pressure. The horizontally lined phase fields include assemblages with melt and equilibrium vapor (gas). The dashed line shows the decompression path for composition **a**. Other symbols are the same as in Fig. 5. See text for further explanation.

the system, the compositions of the melt and vapor phases can reach L_m. The same effect will be observed during the decompression of any other initial melt more oxidized than L_m, i.e., lying right of L_m in Fig. 6. Note that the decompression evaporation of initial reduced iron-rich melts (lying left of L_m in Fig. 6) results in their oxidation. Under open-system conditions, the composition of residual melt will also approach L_m during decompression oxidation.

An increase in the decompression temperature of oxidized melt causes an increase in the pressure of the beginning of incongruent evaporation and, correspondingly, reduction. The pressure of the complete evaporation of melt also increases (Fig. 8). According to approximate estimates based on extrapolations, the incongruent evaporation of a melt similar in composition to hematite at temperatures of 2200 and 2500 K begins at pressures of more than 1000 and 30000 atm, respectively. A pressure decrease to 1 atm under such temperatures leads to the reduction of the major portion of initial oxidized iron in the melt to Fe^{2+}. Note that the higher the temperature, the closer L_m to the composition of stoichiometric wüstite, FeO, i.e., the more reduced the extreme melt composition, to which the initial oxidized melts tend during decompression.

We considered above the cases of decompression reduction at a constant temperature. It is also important to keep in mind that pressure-induced reduction or oxidation reactions must occur not only under isothermal conditions but also at concurrent changes in pressure and temperature, if the trend of P–T variations intersects the lines of redox equilibria in the $\log P - 1/T$ diagram (Fig. 4).

SiO_2–FeO–Fe_2O_3 System

Consider now melts in the SiO_2–FeO–Fe_2O_3 system (Fig. 9). They provide a more realistic model for natural impact melts, which contain SiO_2 as the dominant component (up to 80 wt %) and usually from 1.5 to 5–7 wt % iron oxides. The vapor phase in equilibrium with SiO_2 melt consists mainly (at least up to 3000–4000 K) of SiO and molecular oxygen. The mole fraction of atomic oxygen is no higher than 0.1 under such temperatures, and the concentrations of other components are negligible [63] (Fig. 10). Consider the influence of the addition of an iron oxide mixture with a variable Fe_2O_3/Fe ratio on the composition of the gas phase under isothermal conditions. Figure 11 shows the contents of major components in vapor in equilibrium with melts of the SiO_2–W_m section at 1873 K, where W_m has the composition of congruently evaporating wüstite melt (L_m in Fig. 6). Figure 12b shows similar relations for a higher temperature of 2200 K assuming ideal mixing in the

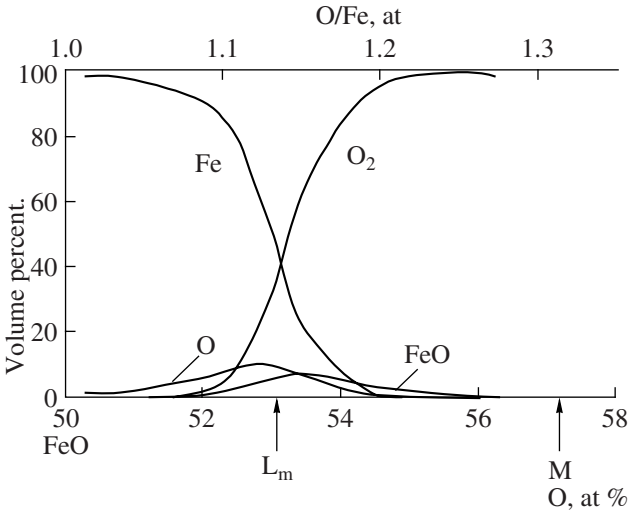

Fig. 7. Composition of vapor phase in equilibrium with iron oxide melts with different oxygen contents at 1870 K according to the data of [64]. M, magnetite; and L_m, iron oxide melt that evaporates congruently upon decreasing pressure.

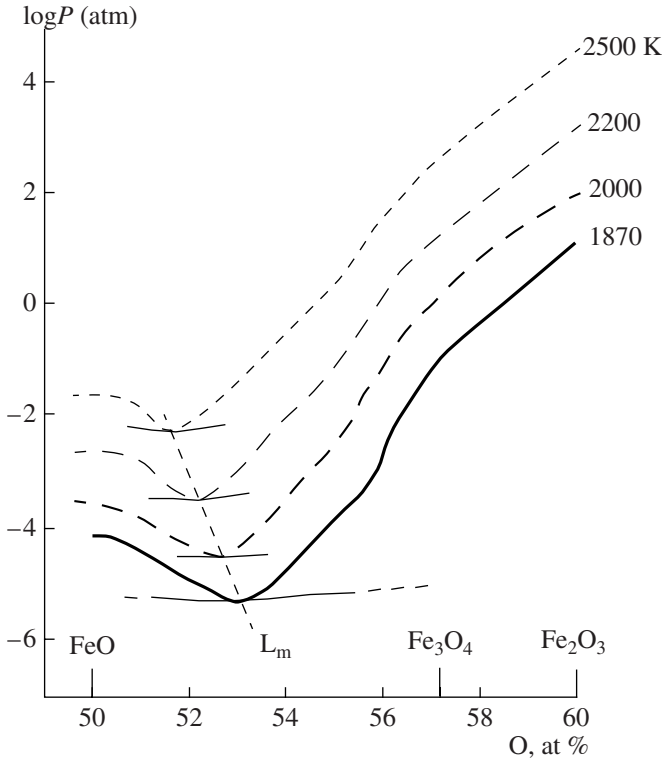

Fig. 8. Total vapor pressure above iron oxide melts of the $FeO–Fe_2O_3$ join at temperatures of 1870–2500 K. The dashed curves are extrapolated from the data on the Fe–O system [64]. The point of minimum pressure P_v corresponds to the composition of melt that evaporates congruently under the given temperature (L_m). The L_m composition shifts toward FeO with increasing temperature.

liquid and vapor phases. With increasing W_m content in the melt, the fraction of atomic iron in the vapor increases at the expense of SiO, while the content of O_2 remains essentially constant at $X(O_2) \sim 0.28–0.29$. When iron oxides corresponding to the magnetite composition (M), which evaporates incongruently producing a vapor enriched in molecular oxygen, $X(O_2) > 0.95$, are added to SiO_2 melt, the relationships change fundamentally. An increase in M concentration in the melt leads to a significant increase in the $X(O_2)$ value of the vapor. The mole fraction of atomic iron in the vapor remains rather small for all iron-bearing compositions of this section (Fig. 12a). The addition of composition W_f, which is more reduced than W_m and corresponds to wüstite in equilibrium with metallic iron under a given temperature, to SiO_2 results in a significant decrease in $X(O_2)$ in the vapor phase, while X(Fe) increases more rapidly than in the case of the addition of W_m (Fig. 12c). Thus, an increase in the Fe_2O_3/FeO ratio of melt (at a constant SiO_2 fraction) is accompanied by a significant change in vapor composition, with the main effect being an increase in O/(Fe + Si).

Similar to the Fe–O system, the described compositional features of vapor phase above the melts of the $SiO_2–FeO–Fe_2O_3$ system provide conditions for changes in the redox state of iron in response to a temperature increase or a pressure decrease. The O/(Fe + Si) ratio of the gas phase formed during the decompression of relatively oxidized melts with Fe_2O_3/FeO ratios higher than that of W_m (lying to the right of the $SiO_2–W_m$ line in Fig. 9) starting from the moment of $P_v = P_{tot}$ must be higher than the O/(Fe + Si) of the melt. As a result, the Fe_2O_3/FeO ratio of melt must decrease with decreasing pressure, i.e., the melt will become progressively more reduced. On the other hand, the decompression evaporation of reduced melts (lying to the left of the $SiO_2–W_m$ line in Fig. 9) must lead to the formation of a vapor with $[O/(Fe + Si)]_{vapor} < [O/(Fe + Si)]_{melt}$ and be accompanied by partial iron oxidation in the melt. Similar to the Fe–O system, the Fe_2O_3/FeO (Fe^{3+}/Fe^{2+}) of melt tends to the limit in which $[O/Fe + Si)]_{vapor} = [O/(Fe + Si)]_{melt}$ during decompression reduction or oxidation. However, it should be noted that for the limiting Fe_2O_3/FeO value for $SiO_2–FeO–Fe_2O_3$ melts and impact melts of more complex compositions will be evidently different from that of Fe–O oxide melts owing to the influence of other components.

The pressure of vapor phase (P_v) above $SiO_2–Fe_xO$ melts depends on the composition of the system and temperature. P_v increases with increasing degree of iron oxidation, iron content in melt, and temperature. Thus, the more oxidized the initial melt and the higher the decompression temperature, the earlier (i.e., at a higher total pressure) the processes of melt evaporation and reduction begin. Approximate estimates of P_v for compositions with a SiO_2 mole fraction of about 0.9 are shown in Fig. 13. Although the fraction of iron oxides in the melt is relatively small, the P_v of oxidized melts may range from a few tens to thousands of atmospheres at high temperatures. For instance, at 2500 K for melts

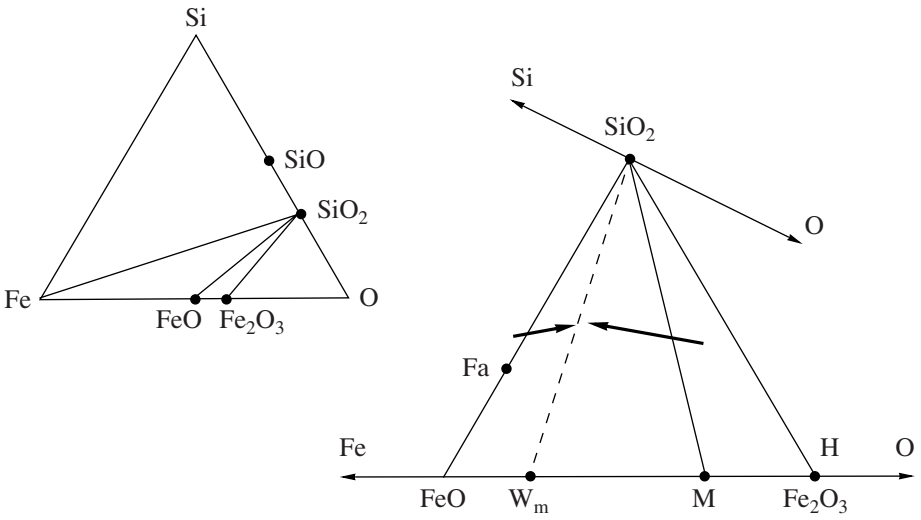

Fig. 9. Compositions of main compounds in the SiO_2–FeO–Fe_2O_3 system and in the more general system Fe–Si–O. Phase abbreviations: Fa, fayalite; W_m, wüstite composition that evaporates congruently under the given temperature (its composition shifts toward FeO with increasing temperature); M, magnetite; and H, hematite. The arrows show variations in the composition and redox state of melts during their evaporation in response to a temperature increase (P_{tot} = const) or a pressure decrease (T = const).

containing the magnetite or hematite component, P_v is ~40 and 3.2×10^3 atm, respectively. In addition to SiO_2, FeO, and Fe_2O_3, natural impact melts may contain other volatile component, the presence of which can lead to a significant increase in P_v. Thus, the pressure range of the evaporation of impact-generated melts can be even more significant under such temperatures.

The above analysis of the processes of melt evaporation in relatively simple systems containing iron in different oxidation states demonstrated that redox reactions inevitably occur in them during high-temperature decompression owing to the incongruent evaporation and variations in partial pressures of components in the gas phase, primarily of O_2 and Fe. This conclusion is obviously valid for more complex natural compositions as well. Calculations performed for the natural compositions of supposed moldavite sources, sedimentary

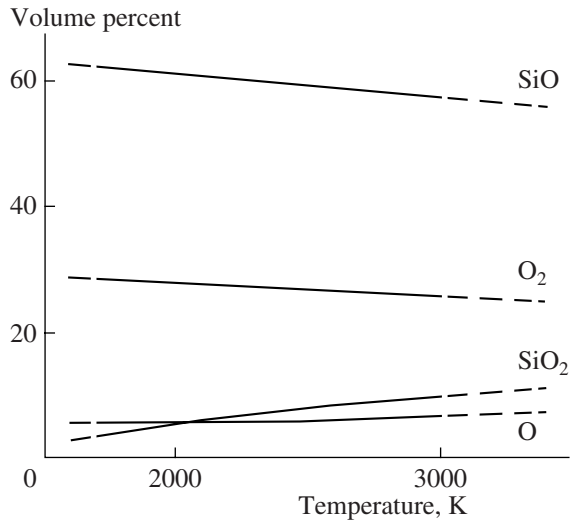

Fig. 10. Influence of temperature on the composition of vapor phase above SiO_2 liquid according to the data of [63].

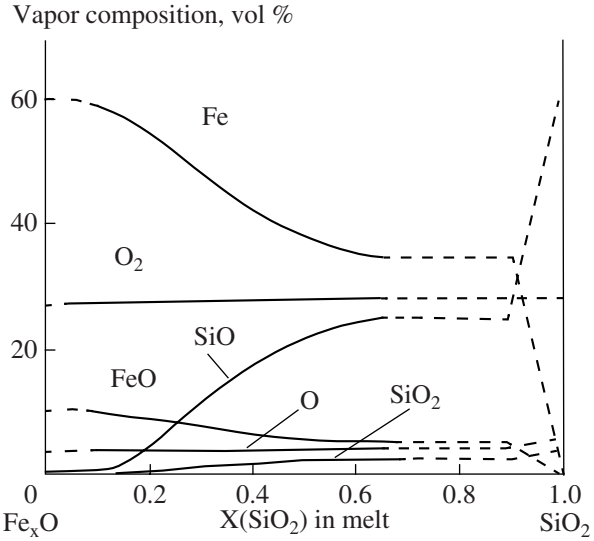

Fig. 11. Variations in the composition of vapor phase above melts in the Fe_xO–SiO_2 system as a function of SiO_2 mole fraction in the melt at T = 1873 K. The diagram shows a section of the SiO_2–FeO–Fe_2O_3 system in which the Fe_xO component is compositionally similar to the iron oxide melt that evaporates congruently under the given temperature. The dashed lines show the approximate compositions of vapor for melts with SiO_2 mole fractions, $X(SiO_2)$, higher than 0.65, i.e., in the compositional interval with a wide liquid immiscibility field under the given temperature.

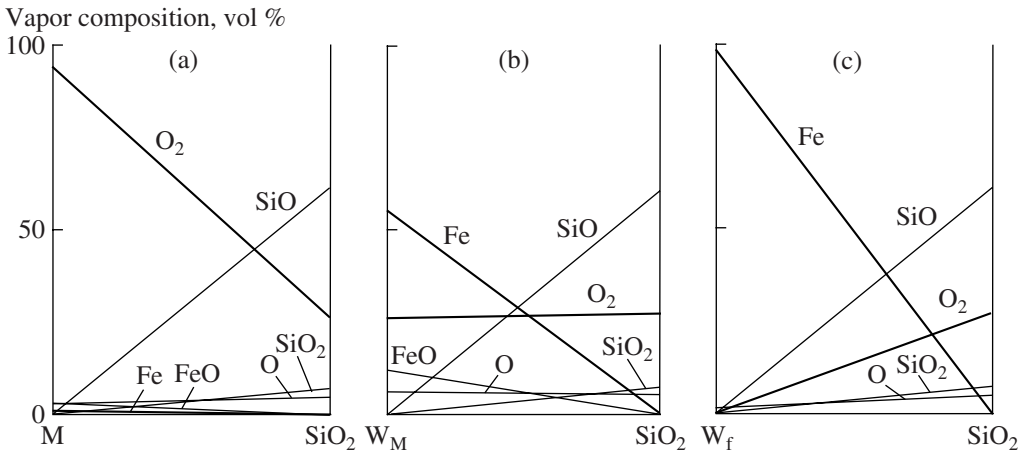

Fig. 12. Composition of vapor phase above Fe_xO–SiO_2 melts at 2200 K. (a) The composition of Fe_xO corresponds to magnetite (M). (b) The composition of Fe_xO corresponds to the oxide liquid evaporating congruently at 2200 K (W_m). (c) The composition of Fe_xO corresponds to the oxide melt of the wüstite composition in equilibrium with metallic iron melt (W_f). The diagrams were calculated on the basis of extrapolations using the data for the Fe–O system [63, 64] and assuming ideal mixing in the liquid and gas phases.

rocks containing only ferric iron, showed that the vapor phase generated under the *P–T* conditions of adiabatic decompression (at temperatures of 6000–2000 K and pressures of 10^4–10^{-3} bar) is enriched in oxygen relative to the equilibrium liquid and starting material [66].

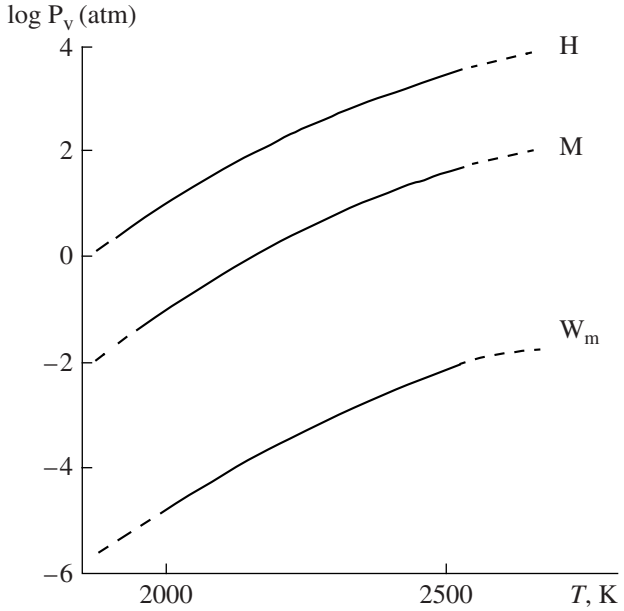

Fig. 13. Variations in vapor pressure (P_v) with increasing temperature for the SiO_2–FeO–F_2O_3 system in equilibrium with a melt with an SiO_2 mole fraction of 0.9. The line labeled H corresponds to the composition in the SiO_2–Fe_2O_3 section in which iron oxide is represented by hematite; the line labeled M corresponds to the composition in the SiO_2–Fe_3O_4 section in which iron oxide is magnetite; and the line labeled W_m corresponds to the composition in the SiO_2–Fe_xO section in which iron oxide is congruently evaporating wüstite.

Thus, it is supposed that the melting and evaporation of materials affected by a strong impact event must produce melts more reduced than the precursor material. The quenching of such melts gives rise to reduced tektite glasses.

Up to now, a number of experimental studies have been carried out on element fractionation during the evaporation and condensation of silicate melts, as a major factor of the chemical differentiation of matter during the formation of planetary bodies [4, 9, 67–74, etc.]. Some of these studies focused on the elucidation of the character of chemical transformations during impact and explosion processes [4, 9, 68, 73]. In the next section, we consider the most important results of these studies that have a direct bearing on the problem of iron oxidation state in tektites and impactites.

MEASUREMENT OF IRON OXIDATION STATE IN EXPERIMENTS ON THE HIGH-TEMPERATURE EVAPORATION OF SILICATE MELTS

Various approaches have been used for the experimental simulation of vaporization and condensation processes. For our purposes, of special interest are vaporization experiments in vacuum or in a neutral medium and experimental reproduction of the evaporation and condensation of materials during impactor–target interactions using a metallic impactor or a laser pulse.

Evaporation of Silicate Melts in Vacuum or an Inert Medium

Most experiments on the evaporation of silicate melts in vacuum were conducted at a total pressure of 10^{-4}–10^{-8} atm temperatures of 1600–2100°C [67, 68,

70, 72]. In some cases, evaporation was modeled under ambient pressure in an inert gas (argon) atmosphere [69]. Vapor phase was condensed on special plates mounted in the cold parts of the reaction chamber. After the experiments, the degree of evaporation of the initial material and the composition of residual melt were determined. When possible, the condensate was also analyzed. The starting materials were represented by natural and synthetic melts of complex compositions, with significant variations in iron content and oxidation state. Such experiments simulated dynamic evaporation, i.e., both evaporation and condensation occurred concurrently. Part of the vapor phase, primarily its most volatile gas components, could be lost during condensation. Thus, the composition of vapor estimated on the basis of these results does not correspond to equilibrium conditions. Evaporation experiments in a Knudsen cell apparatus [71] provide more reliable information on the composition of a vapor phase in equilibrium with melt. However, even in such a case, the composition of the vapor phase may be modified by interaction with the materials of experimental setup (container, heater, etc.). This factor must be accounted for during the estimation of the partial pressures of components in vapor and, especially, of such an important parameter as oxygen partial pressure.

Figure 14 summarizes the results of experiments in which the Fe^{3+}/Fe^{2+} ratio of melts was determined after their partial evaporation. At first glance, the experimental results are controversial: evaporation may be accompanied by both reduction and oxidation of iron in the melt. However, a more detailed analysis allowed us to reveal some features that can be explained on the basis of phase relations in the Fe–O and SiO_2–FeO–Fe_2O_3 systems considered above.

In all of the experiments with silicate melts in which the fraction of ferric iron was high, partial reduction was observed during evaporation. During the evaporation in argon at 1 atm of initial silica-rich melt corresponding to moldavite in major-element composition but containing mostly ferric iron, Fe^{3+} was almost completely reduced (1 in Fig. 14) [69]. The resulting $Fe^{3+}/\Sigma Fe$ values of the experimental melts approached the level of typical tektites. Partial reduction of Fe^{3+} was also observed in experiments on the evaporation in vacuum of basalts with initial $Fe^{3+}/\Sigma Fe \geq 0.3$ (3 and 4 in Fig. 14) [68]. The analysis of condensates from these experiments revealed the presence of metallic iron, which was absent in residual melts.

When reduced melts, in which all or nearly all iron was Fe^{2+}, were used as starting materials in evaporation experiments, the residual melt showed partial oxidation of iron. In particular, the oxidation of residual melts in the FeO–MgO–SiO_2–CaO–Al_2O_3 system [70, 72] resulted in the appearance of magnetite crystals among the phases formed during melt quenching (4 in Fig. 14). The same tendency toward ferrous iron oxidation was observed in experiments on the evaporation of the natural melt of a philippinite tektite (2 in Fig. 14) [67].

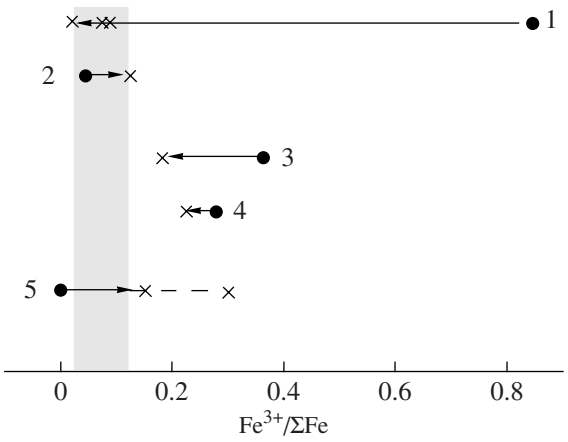

Fig. 14. Variations in $Fe^{3+}/\Sigma Fe$ during the evaporation of silicate iron-bearing melts according to experimental data. Circles show the $Fe^{3+}/\Sigma Fe$ values of initial melts, and crosses are $Fe^{3+}/\Sigma Fe$ values of residual melt after experiments. The arrows indicate variations in the degree of iron oxidation in the residual melt during evaporation. The shaded area corresponds to the $Fe^{3+}/\Sigma Fe$ values of tektite gasses (Fig. 1). Tektite melts: 1—model melt of initial moldavite composition obtained by melting of natural shales (SiO_2 = 73.2 wt %, FeO_t = 2.0 wt %, T = 1700–2100°C, and P_{tot} = 1 atm Ar) [69] and 2—melt of natural tektite-philippinite (SiO_2 = 70.6 wt %, FeO_t = 4.8 wt %, T = 2060–2090°C, and $P_{tot} = 10^{-3}$ mm Hg) [67]. Basaltic melts (T = 1700 and 1600°C at $P_{tot} = 2 \times 10^{-2}$ mm Hg) [68]: 3—iron-rich basalt from northern Tanzania (SiO_2 = 43.3 wt % and FeO_t = 14.6 wt %); 4—basalt from Klyuchevskoy Volcano, Kamchatka (SiO_2 = 52.2 wt % and FeO_t = 8.8 wt %); and 5—synthetic composition in the FeO–MgO–SiO_2–CaO–Al_2O_3 system (SiO_2 = 35.4 wt %, FeO_t = 35.0 wt %, T = 1800°C, and $P_{tot} = 10^{-5}$ mm Hg) [70].

Thus, it can be seen that the direction of redox reactions accompanying evaporation (similar to the Fe–O and SiO_2–FeO–Fe_2O_3 systems) depends on the degree of iron oxidation in the initial melt. The evaporation of oxidized initial melts leads to the reduction of ferric iron, which results in that the vapor phase is relatively enriched in oxygen and the O/(Fe + Si + Al + other cations) value of the vapor is higher than that of the residual melt. In contrast, reduced initial melts are partly oxidized during evaporation, because the released vapor phase is relatively enriched in atomic iron and its O/(Fe + Si + Al + other cations) ratio is lower than that of the melt. As was shown above by the example of simple iron-bearing systems, the O/(Fe + Si + Al + other cations) ratios of vapor and melt phases may converge during equilibrium evaporation under open-system conditions and become equal at a certain moment. After that, further evaporation must not affect the Fe^{3+}/Fe^{2+} value of the residual melt. It should be noted that in the case of complex silicate melts, such limiting Fe^{3+}/Fe^{2+} values can be significantly dependent both on melt composition and P–T conditions. It should also be taken into account that the chemical compositions of

melts change significantly during evaporation owing to the selective vaporization of major components. Therefore, the limiting Fe^{3+}/Fe^{2+} values in residual melts may vary to some extent during evaporation. In the experiments considered above, evaporation processes were modeled for melts of different compositions at various *P–T* parameters under far-from-equilibrium conditions. This is probably why the residual melt from all these experiments could not tend to the same universal Fe^{3+}/Fe^{2+} value during evaporation.

Hashimoto [70] argued on the basis of his experimental data that the main reason for the oxidation of ferric iron is the preferential vaporization of atomic Fe relative to oxygen. He suggested that Fe^{2+} can be oxidized in melt via the following disproportionation reaction:

$$3Fe^{2+}(melt) = Fe^{0}(metal) + 2Fe^{3+}(melt). \quad (1)$$

Thus, tiny inclusions of metallic iron must be present in the melt. These metal inclusions occur as a transitional phase and disappear during melt cooling probably owing to the rapid reverse reaction (metal phase was not found in quenched products).

Melt Evaporation in Impact Simulation Experiments. There is little experimental data in this field [4, 9, 73, 74]. We mention here only those results that have a direct bearing on the change of the oxidation state of iron and other elements during the vaporization and condensation of silicate materials. In this context, of particular importance are experiments in which the occurrence of redox reactions during evaporation is not affected by the presence of strong reducers, such as metal or graphite, in the impactor and/or target materials. Very instructive are experiments on the evaporation of iron-bearing silicate materials under the influence of pulsed laser irradiation, which were conducted in an inert gas (helium) atmosphere at 1 atm. Temperatures of about 4000°C were reached in these experiments, providing evaporation under near equilibrium conditions. The analysis of condensates from these experiments revealed the presence of both Fe^{2+}, Fe^{3+}, and zero-valence iron. In addition to Fe^{0}, the reduced species of other elements were detected: Al^{0}, Si^{0}, Si^{2+}, etc., the fraction of which is usually no higher than ~10 at % of the total content of the given element. Layer-by-layer analysis revealed variations in the proportions of reduced and oxidized species of iron and other elements with depth in the condensate film, which is related to the kinetics of the condensation process [73, 74]. The investigation of a vapor cloud generated during pulse evaporation suggests that the vapor composition is rich in free oxygen, part of which remains in an unbonded gas state after the condensation of the vapor phase. This is in good agreement with the Knudsen cell mass spectrometry of vapors above silicate melts [71] and with thermodynamic calculations [75].

Yakovlev et al. [73] reported experiments on the laser evaporation of the analogs of lunar rocks with some carbonaceous chondrite material and observed melt drops quenched to glass spherules in the condensates. These melts were evidently ejected from the crater hollow of the sample. Microscopic globules of metallic iron were observed on the surface of some spherules. It was suggested that their formation was related to liquid immiscibility phenomena in the melt and the kinetics of reduction owing to the preferential evaporation of zero-valence iron from the melt. If this is the case and the formation of metallic iron in melt was not due to the presence of a reducer (admixture of carbonaceous matter) in the target material, it can be concluded that the observed quenched phase corresponds to a transitional stage of melt evaporation with the formation of metallic iron similar to that proposed previously by Hashimoto [70]. On the other hand, there is another viable mechanism for the formation of iron microglobules by the condensation of the gas phase, which was observed in melt evaporation experiments [68].

Summarizing the available experimental data, it can be concluded that the processes of high-temperature evaporation of complex silicate melts are selective and cause changes in the oxidation state of iron and other elements. Iron and some other elements may occur in a zero-valence state in a vapor phase. The presence of reduced element species in a vapor is manifested during its rapid nonequilibrium cooling: the reduced species of iron and other elements were also observed in the condensate produced from the vapor. Evaporation also induces changes in the oxidation state of iron in the residual melt. The occurrence of evaporation-related oxidation (increase in Fe^{3+}/Fe^{2+}) or reduction (decrease in Fe^{3+}/Fe^{2+}) in melts is controlled by the redox state of the initial material. During the evaporation of initially both oxidized and reduced compositions, the Fe^{3+}/Fe^{2+} value of residual melts probably tends to a certain limiting value, which depends on the composition of melt and *P–T* conditions of evaporation. Evidence on simple iron-bearing systems suggests that the higher the temperature, the lower the limiting Fe^{3+}/Fe^{2+} value. The experimental data discussed above suggest also that the rapid cooling of a melt–vapor mixture may produce a quench phase (melt + condensate) containing elements with different oxidation states, including zero-valence species of iron and other elements.

INFLUENCE OF *T-P-*pO_2 PARAMETERS ON THE Fe^{3+}/Fe^{2+} VALUE OF IMPACT MELTS

There are extensive experimental data on the influence of *T-P-*fO_2 parameters on the Fe^{3+}/Fe^{2+} ratio of natural silicate melts of various compositions and electrochemical measurements of pO_2 for natural tektite glasses with known Fe^{3+}/Fe^{2+} ratios. Using these data, let us consider possible relations between temperature, total pressure, oxygen partial pressure, and Fe^{3+}/Fe^{2+} in silicate melts produced by impact events.

Model

As a first approximation, it can be assumed that, similar to other iron-bearing silicate melts, the $pO_2 = f(T, P)$ dependence for tektite and other impact melts of a given composition with a constant value of $R_i = Fe^{3+}/Fe^{2+}$ within a wide range of T–P parameters has the same form as that for solid-state buffer equilibria, like fayalite–magnetite–quartz (FMQ), magnetite–wüstite (MW), iron–quartz–fayalite (IQF), etc.:

$$\log(pO_2) = a_i - b/T + c(P_{tot} - 1)/T, \qquad (2)$$

where a_i, b, and c are the coefficients. The value of a_i depends on the R_i of the melt. If $R_1 > R_2$, then $a_1 > a_2$, i.e., the higher the Fe^{3+}/Fe^{2+} ratio of melt, the higher pO_2 under given T and P.[3]

The above assumption can be justified by the following data. First, there is experimental and theoretical evidence for the influence of T and P on the valence state of iron in igneous melts. The dependence of melt Fe^{3+}/Fe^{2+} on pO_2, T, and major element contents in melts is well described at 1 atm by empirical relationships [76–78]. These relations suggest that for a given melt composition with a constant Fe^{3+}/Fe^{2+} ratio, variations in pO_2 as a function of temperature (at least up to 1400–1550°C) are similar to those of buffer equilibria, such as FMQ and MW, i.e., they can be described by Eq. (2) with b values similar to the respective coefficients of the FMQ and MW buffer equilibria. Experimental data on the volume effect of the $Fe^{3+} \longrightarrow Fe^{2+}$ transition in silicate melts [79] and pressure influence on Fe^{3+}/Fe^{2+} under closed-system conditions [80] indicate that, within a wide range of P–T parameters, an increase in pO_2 with increasing P_{tot} (at constant T and Fe^{3+}/Fe^2 in the melt) approximately parallels the pO_2–P_{tot} curves of the FMQ and MW buffer equilibria, i.e., the coefficient c in Eq. (2) for iron-bearing silicate melts is similar to that describing the FMQ and MW buffer equilibria. The coefficient a of Eq. (2) depends on the oxidation state of iron in the melt and, in the more general case, on the concentrations of all other components. The value of a can be estimated from the available empirical relations for the melts of basalt and basaltic andesite compositions [78]. However, these relations are not valid for felsic melts. Therefore, the values of a cannot yet be reliably constrained for tektite and impactite melts.

Another compelling argument supporting the above assumption comes from the results of electrochemical measurements of intrinsic oxygen fugacity for tektite glasses (moldavites and indochinites), which were carried out at 1 atm and temperatures of 800–1150°C. They showed that the $\log(pO_2)/\Delta(1/T)$ slope for tektites is very similar to that of the MW buffer, and the lines of tektites approximately parallel the MW curve in the $\log(pO_2)$–$1/T$ diagram. The absolute values of pO_2 for the majority of tektites studied are 1.5–2.0 orders of magnitude lower than pO_2(MW) at the same temperature [10, 31, 32] (e.g., Fig. 1 in [10]).

Thus, pO_2 variations can be described to a first approximation as a function of temperature, pressure, and Fe^{3+}/Fe^{2+} ratio in tektite and impactite melts using expressions similar to Eq. (2), where the coefficients b and c are similar to the respective parameters for the MW buffer. The above assumptions imply that the $pO_2 = f(T, P)$ dependencies for impactite melts of certain compositions with constant Fe^{3+}/Fe^{2+} ratios parallel the lines of the MW buffer equilibrium in the $\log(pO_2)$–$1/T$ and $\log(pO_2)$–$\log(P_{tot})$ diagrams. The value of a equals $\log(pO_2)$ for a melt with the given $Fe^{3+}/Fe^{2+} = R_i$ minus $\log(pO_2)$ (MW), i.e., it corresponds to the difference in logarithmic units between the pO_2 values of the impact melt and the MW buffer at a given temperature. Using the accepted model, consider some principal characteristics of variations in pO_2 and iron oxidation state in impact melts in response to changes in the P–T parameters of the system.

Thermal Reduction

Figure 15 presents schematic relations between T and pO_2 for a model melt similar in major-element composition to tektites and felsic impactite glasses. Lines R_1–R_5 parallel to the MW buffer show pO_2 variations with temperature for this melt at different Fe^{3+}/Fe^{2+} ratios. Compositions R_1, R_2, and R_3 have relatively high Fe^{3+}/Fe^{2+} ratios, corresponding to those of the target rocks (≥0.2–0.3), and R_4 and R_5 are melts with Fe^{3+}/Fe^{2+} values typical of tektites (≤0.12). Similar to the Fe–O and SiO_2–FeO–Fe_2O_3 systems, relatively oxidized initial melts can be reduced upon heating or high-temperature decompression. Indeed, under closed-system conditions, the values of P_v and pO_2 above melts with constant $Fe^{3+}/Fe^{2+} = R_1$ increase during isobaric heating and approach P_{tot}. For strongly oxidized initial melts, molecular oxygen is the main component of the vapor phase and pO_2 approaches P_v. When the condition $P_v = P_{tot}$ is met (in the case shown in Fig. 15, at $P_{tot} = 10^{-2}$ bar), a further increase in temperature under equilibrium conditions will be accompanied by a gradual reduction of Fe^{3+} in the melt and a corresponding decrease in Fe^{3+}/Fe^{2+} from R_1 to R_5 (trend shown by arrows in Fig. 15). The value of pO_2 will decrease owing to an increase in the fraction of atomic iron and other components in the vapor. By analogy with simple iron-bearing systems, it can be suggested that, owing to an increase in pFe in the vapor with increasing temperature, a limiting value of melt Fe^{3+}/Fe^{2+} (R_m) can be attained, after which the degree of iron oxidation in the melt remains invariant during further evaporation. The data for the Fe–O system suggest

[3] In Eq. (2) for buffer equilibria, oxygen fugacity (fO_2) is often used instead of pO_2. Hereafter, we assumed $pO_2 = fO_2$, which is a reasonable approximation for high temperatures and relatively low pressures and does not affect the results of analysis under the assumptions discussed above.

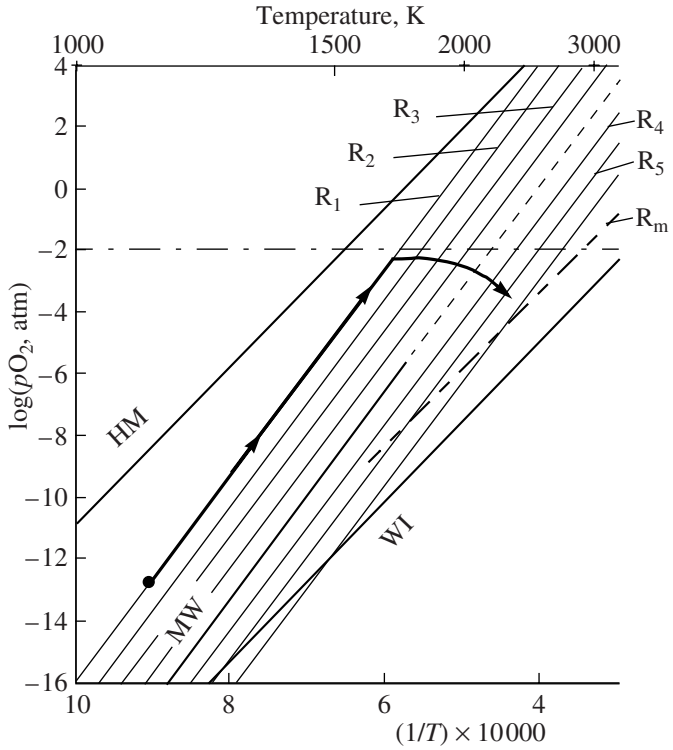

Fig. 15. Diagram showing the mechanism of thermoreduction of iron-bearing silicate melts of the tektite composition during their heating at a constant total pressure. MW and FMQ are the magnetite–wüstite and fayalite–magnetite–quartz buffer equilibria, respectively. Lines R_1, R_2…R_5 show pO_2 variations for melts with different Fe^{3+}/Fe^{2+} ratios. The bold line with arrows shows the trend of pO_2 changes with increasing temperature for a melt with the initial ratio $Fe^{3+}/Fe^{2+} = R_1$ under a constant total pressure of $P_{tot} = 10^{-2}$ atm. Other symbols are the same as in Fig. 4. See text for further explanation.

that the pO_2 values corresponding to R_m must be about 2–3 orders of magnitude below pO_2(MW) (Fig. 15).

The extent of iron reduction in melts during heating under closed-system conditions is a function of both temperature and total pressure. The lower the P_{tot} in the system, the lower the temperature at which the condition $P_v(\approx pO_2) = P_{tot}$ is met and partial reduction of Fe^{3+} begins during the heating of oxidized initial melts. The low Fe^{3+}/Fe^{2+} values (close to R_4 and R_5) of reduced melts generated at high temperatures can be retained in quenched glasses in the case of a rapid nonequilibrium cooling with simultaneous decreases in P_{tot} and pO_2, when interaction with the gas phase is strongly depressed, or under open-system conditions, when the gas phase is removed from the system.

Decompression Reduction. In contrast to heating at a constant pressure discussed above, impact melting and evaporation are accompanied by a pressure decrease under adiabatic (isentropic) conditions. Therefore, the possibility of the decompression reduction of silicate melts generated by impact events deserves special attention. The temperature of material after unloading (residual temperature) depends on the initial pressure of the shock wave. The higher the pressure, the higher the temperature at the unloading stage [1, 2]. If temperature values characteristic of tektite melt formation (≥1800–2000°C) are reached during decompression, further pressure release will inevitably trigger reduction reactions involving iron and other elements, which will be demonstrated below. Consider the main factors controlling the oxidation state of iron during adiabatic decompression.

Figure 16 shows schematic pO_2 variations for a model impact melt as a function of total pressure, temperature, and melt Fe^{3+}/Fe^{2+} ratio under the above assumptions. The P_{tot} interval corresponds to the formation of tektites and impactites during the final stages of release after strong shock compression [1, 2]. Let the temperature of totally molten material be ≅2250°C at a pressure of more than 30–40 kbar during the unloading stage. The Fe^{3+}/Fe^{2+} ratio of the melt is taken to be equal to the pO_2 value of the MW buffer (in our notation, Fe^{3+}/Fe^{2+} = R(mv); Fig. 16). The adiabatic gradient of silicate melt is ≈1°C/kbar [81]. As a first approximation, the initial stages of adiabatic decompression, when the mass of condensed phases is much higher than that of the gas phase, can be considered as isothermal. With decreasing P_{tot}, the $\log(pO_2)$ value of melt with Fe^{3+}/Fe^{2+} = R(mv) follows a trend shown in Fig. 16, and the difference between pO_2 and P_{tot} decreases. At point *b* (Fig. 16b), the vapor pressure becomes equal to the total pressure, and a further decrease in P_{tot} will cause melt evaporation, which is accompanied by a decrease in pO_2 in the system and, correspondingly, partial reduction of Fe^{3+}. The value of P_v for this model melt is not known, and the position of point *b* cannot be determined. The value of P_v can be roughly estimated using the data for the SiO_2–FeO–Fe_2O_3 system. At a constant melt SiO_2 content, the higher the Fe^{3+}/Fe^{2+} ratio of the melt, the greater the fraction of molecular oxygen in the vapor, the smaller the difference between pO_2 and P_v, and, correspondingly, the closer point *b* must lie to points *a* and *c* (Fig. 16b). With decreasing Fe^{3+}/Fe^{2+} in the melt, the fraction of O_2 in vapor decreases, but even in this case, pO_2 is no lower than 0.3–0.5 of P_v (Figs. 11 and 12). Thus, P_v can be about 2–3 times higher than pO_2 for relatively reduced melts. It should be kept in mind that, owing to the presence of other volatile components, the fraction of O_2 in the vapor coexisting with natural melts can be significantly lower than in the vapor phase of the SiO_2–FeO–Fe_2O_3 system. Despite the above-described uncertainties in the estimation of the onset of evaporation, there is a definite tendency in variations in the degree of melt oxidation during isothermal decompression: as P_{tot} decreases below the value corresponding to the condition $P_v = P_{tot}$ (point *a* in Fig. 16b), pO_2 and, correspondingly, Fe^{3+}/Fe^{2+} in the

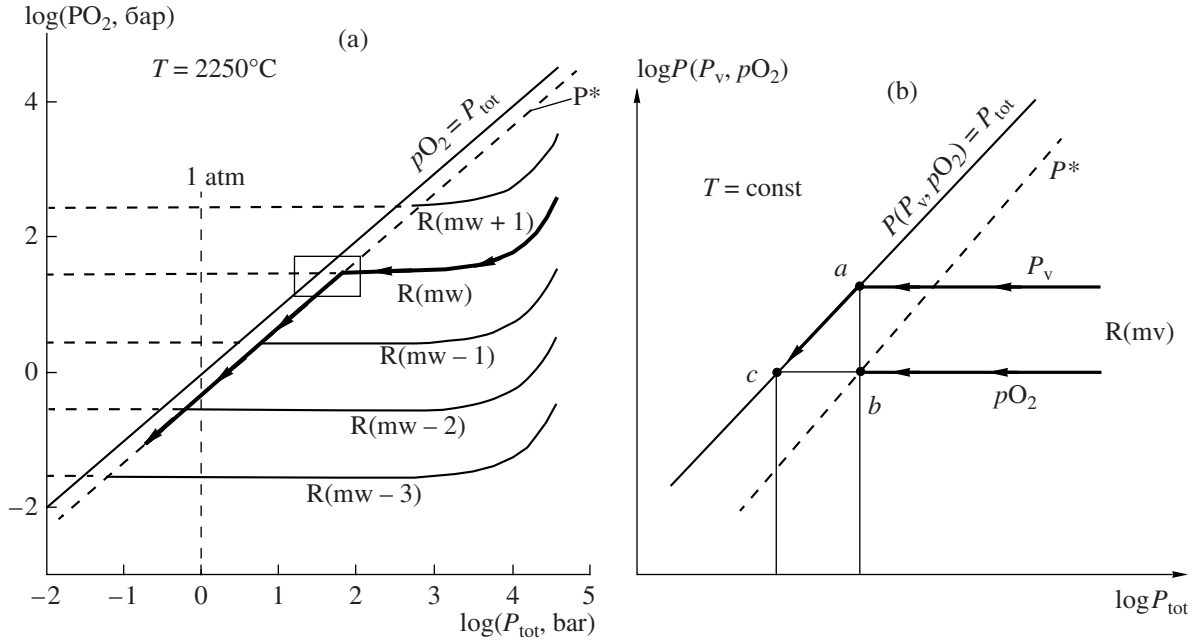

Fig. 16. (a) Variations in pO_2 as a function of total pressure (P_{tot}) for melts with various Fe^{3+}/Fe^{2+} ratios under isothermal conditions (T = 2250°C). R(mw) and R(mw ± n) are the Fe^{3+}/Fe^{2+} ratios in melt at pO_2 values corresponding to the MW buffer or n logarithmic units above or below the MW buffer. The bold lines with arrows show pO_2 variations during the isothermal decompression of initial melt with Fe^{3+}/Fe^{2+} = R(mw). The area within the rectangle is schematically shown at a larger scale in Fig. 16b. (b) Schematic diagram showing pO_2 variations during the isothermal decompression of melt with Fe^{3+}/Fe^{2+} = R(mv). Point *a* corresponds to the condition $P_v = P_{tot}$, when the pO_2 value corresponds to pressure in point *b*. Point *c* corresponds to the conditions when the vapor phase consists of O_2 only and, correspondingly, $P_v = pO_2 = P_{tot}$. The dashed line labeled P* is the locus of points *b* for melts with various Fe^{3+}/Fe^{2+} ratios. It shows the pO_2 values under which the condition $P_v = P_{tot}$ is met and subsequent P_{tot} decrease results in a decrease of both P_v and pO_2 in the system. See text for further explanation.

melt decrease. At P_{tot} < 1.0–0.5 atm, the melt Fe^{3+}/Fe^{2+} ratio approaches R(mv-2) (Fig. 16a), i.e., the ratio corresponding to the pO_2 value two orders of magnitude lower than pO_2(MW) under the given temperature. Note that similar pO_2 values were estimated for tektite melts on the basis of electrochemical measurements [10, 31, 32].

Under a given temperature, the higher the initial Fe^{3+}/Fe^{2+} ratio of the melt, the higher the pressure at which the condition $P_v = P_{tot}$ is met during decompression and melt evaporation and reduction begin. On the other hand, the higher the initial temperature of a melt with the given Fe^{3+}/Fe^{2+} ratio, the higher the total pressure at which the condition $P_v \cong P_{tot}$ can be satisfied, and the more significant is the relative reduction of the melt during isothermal and adiabatic decompression to a certain pressure value. As can be seen from Fig. 17, during the decompression of *R*(mv) melts at temperatures below 1750°C, the trend of pO_2 variations intersects the *P** line corresponding to the attainment of the $P_v = P_{tot}$ condition only at rather low pressures of $<10^{-2}$ bar. Thus, the decompression of relatively low-temperature impact melts is not accompanied by Fe^{3+} reduction up to fairly low P_{tot} values, which can hardly be observed during impact processes.[4]

DISCUSSION. A SIMPLIFIED SCENARIO FOR VARIATIONS IN Fe^{3+}/Fe^{2+} DURING IMPACT MELT FORMATION

The main features of changes in the redox state of iron in impact melts can be viewed in a generalized form in Fig. 18. This diagram presents the *P–T* conditions of impact melt evaporation depending on the initial Fe^{3+}/Fe^{2+} ratio. The lines designated R(mw ± n) correspond to the *P–T* parameters at which the condition $P_v = P_{tot}$ is met for melts with Fe^{3+}/Fe^{2+} = R(mw ± n) at a pO_2 value differing by n orders of magnitude from pO_2(MW). Since molecular oxygen is one of the main components of the vapor phase coexisting with iron-bearing aluminosilicate melts, these lines were calculated assuming that, to a first approximation, $P_v \cong pO_2$.

[4] The Fe^{3+}/Fe^{2+} ratio of melt will not change only if decompression will be accompanied by a considerable decrease in temperature. For the case shown in Fig. 17, when the initial melt shows Fe^{3+}/Fe^{2+} = R(mw) at 2250°C, the redox state of iron must not be significantly modified if a change in P_{tot} from 100 to 1 atm is accompanied by a temperature decrease by more than 250°C.

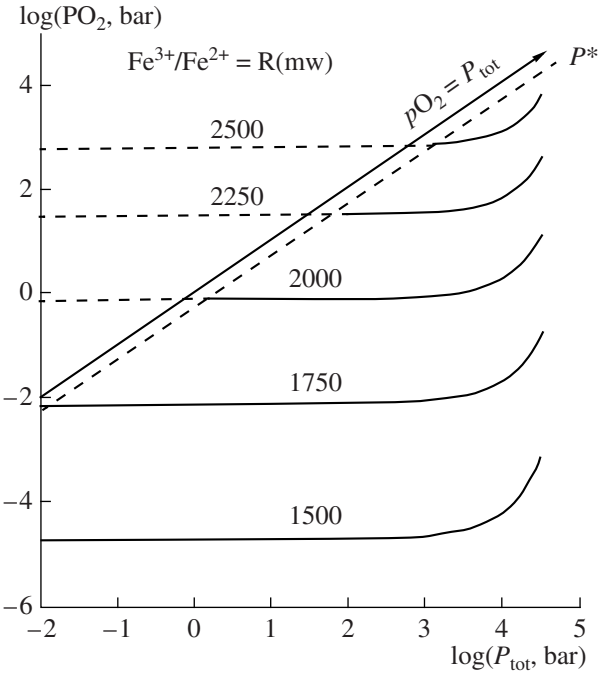

Fig. 17. Isotherms of pO_2 variations as a function of total pressure for a melt with constant Fe^{3+}/Fe^{2+} = R(mw). Numbers indicate temperatures in degrees Celsius. The intersection point of the pO_2 isotherm with line P* corresponds to the moment at which the condition $P_v = P_{tot}$ is met. See text for further explanation.

In general, although the position of R(mw ± n) curves is not precisely known, especially for reduced melts (pressure of the onset of evaporation at a given temperature appeared to be somewhat underestimated), the presented scheme adequately reflects the main features of the evolution of the redox state of iron during impact melt formation.

Consider the case when an initial impact melt is formed from a relatively oxidized target material and shows Fe^{3+}/Fe^{2+} = R(mw + 2). This proportion does not change within the whole superliquidus *P–T* region bounded at high temperatures by the R(mv + 2) line. Melt evaporation must occur above this line, which changes the Fe^{3+}/Fe^{2+} value of melt. Figure 18 shows several possible paths of adiabatic decompression for melts with identical initial Fe^{3+}/Fe^{2+} values of R(mw + 2) and different temperatures at $P_{tot} = 10^4$ (lines 1–4 with arrows). Line 1 corresponding to a temperature of 1700°C at 10 kbar does not intersect line R(mw + 2) within the whole pressure range up to fairly low values of $P_{tot} < 10^{-1}$–10^{-2} bar, which indicates the absence of reduction along this path. The Fe^{3+}/Fe^{2+} ratio of melt does not change within this pressure range. The paths of higher temperature melts with initial temperatures of ≥2000°C intersect the R(mw + 2) line at various P_{tot} values (points *a*, *b*, and *c* in Fig. 18), which increase significantly with increasing temperature from ~5 bar at 2000°C (point *a*) to 2500 bar at 2750°C (point *c*). Adiabatic decompression below the intersection with the R(mw + 2) line results in a decrease in pO_2 and partial reduction of Fe^{3+} in the melt. As P_{tot} decreases to 1 atm, pO_2 decreases by more than an order of magnitude for a melt with an initial temperature of 2000°C (line 2) and by approximately four orders of magnitude for a melt with an initial temperature of 2500 °C (line 4). In general, the higher the temperature and the degree of oxidation of impact melt, the higher the pressure of the beginning of melt evaporation, and the more pronounced reducing effect can be achieved during melt decompression.

If the temperature of melt is higher than 2300–2500°C at $P_{tot} = 10^4$ bar, a significant portion of melt can be transformed into a gaseous state at low pressures during the final stages of decompression. The transitional *P–T* region (Fig. 18), where a complex silicate melt is completely evaporated (or its condensation begins), is bounded by the boiling (condensation) curves of SiO_2 and Al_2O_3, which are the main components of aluminosilicate melts. In addition, the calculated boiling curve of forsterite liquid is shown in Fig. 18 after [2]. As a high-temperature impact melt approaches this region, a considerable portion of the melt is transformed into the gaseous state. A significant increase in the gas/liquid proportion in the system results in an increase in adiabatic temperature gradient and a dramatic change in the adiabat path. As a result, the magnitude of decompression cooling increases significantly and the opposite process can be observed at a certain stage of decompression, when the vapor phase is condensed to form liquid and solid phases.

A melt with a temperature of 3500°C at 10 kbar experiences significant evaporation during the decompression stage at pressures of lower than 200–150 bar with a sharp increase in the fraction of vapor phase in the system (line 6 in Fig. 18). Under such conditions, the Fe^{3+}/Fe^{2} ratio of the melt must correspond to the pO_2 value 2.0–2.5 orders of magnitude lower than pO_2(MW), irrespective of the initial redox state of the target material. During further decompression, the slope of the adiabatic path will approach the slope of the evaporation (condensation) curves of silicate melts and, correspondingly, R(m ± n) lines. This means that the Fe^{3+}/Fe^{2+} of melt will not vary significantly during decompression.

The temperatures of shock-affected materials may be >5000°C during strong impacts [1, 2, 4]. Thus, they can occur completely or partly in a gaseous state at a certain stage of decompression at pressures of several tens of kilobars. Figure 18 shows two examples of adiabatic decompression paths for a material of the moldavite composition formed at the expense of Miocene sandstones similar to those occurring near the Ries impact crater. The calculations were carried out for two values of specific entropy of 5000 and 7500 J/kg K [66]. In both cases, the material is represented by a gas–liquid mixture. The calculated M_2 trend passes close to

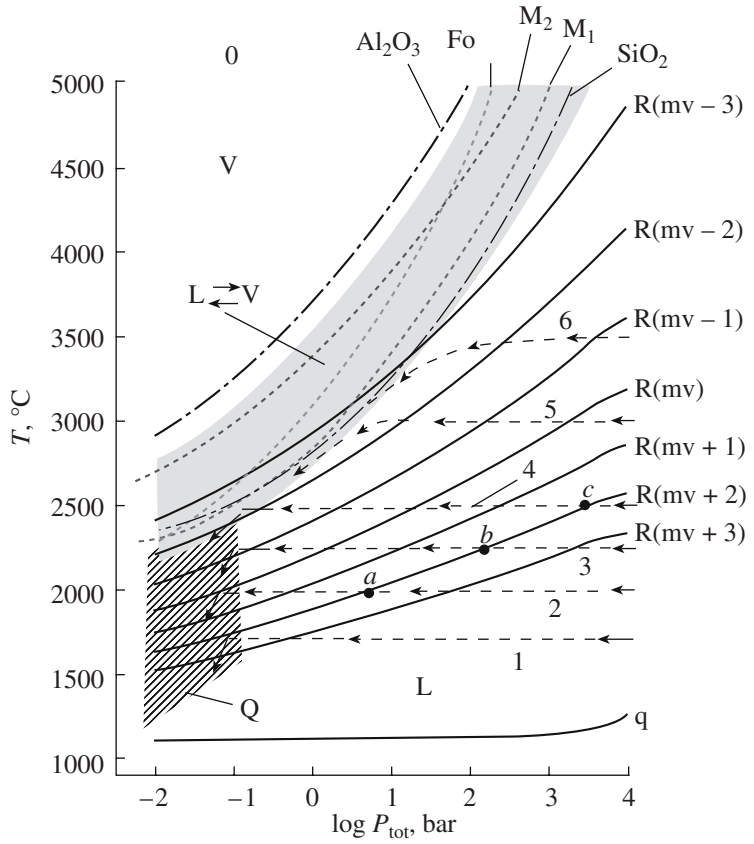

Fig. 18. Generalized relationships illustrating changes in the redox state of impact melts during their adiabatic decompression. Abbreviations: L, melt; V, vapor; and Lq, liquidus line for the granitoid silicate material. Lines R(mw), R(mw ± n) correspond to the condition $pO_2 = P_{tot}$ for melts with constant Fe^{3+}/Fe^{2+} ratios at pO_2 equal to pO_2(MW) and n orders of magnitude higher or lower than pO_2(MW), respectively. Dashed lines with arrows 1–6 are the adiabatic decompression paths of impact melts. The dash–dot lines are the boiling (condensation) curves of SiO_2 and Al_2O_3 melts. The dashed lines show the paths of L + V equilibria during the adiabatic decompression of silicate materials having forsterite composition (Fo) [2] and moldavite composition calculated for two values of specific entropy, 5000 (M_1) and 7500 J/kg K (M_2) [66]. The shaded field labeled L ⇄ V is the *P–T* region of the complete transformation of liquid silicate material to a vapor state (or, correspondingly, the region of the beginning of vapor condensation and melt formation). The hatched field labeled Q is the region of quenching of a melt–gas mixture and generation of impact glasses. See text for further explanation.

the boundary of complete evaporation for the moldavite material.

The calculations and analysis of particular cooling paths of silicate vapor phase or liquid + vapor mixture in the impact process are beyond the scope of this paper. We note only one important consequence of the above-discussed relations. Independent of the initial oxidation state of the target rocks, the melts that are generated in the melt–gas transitional region at pressures of lower than 10–20 kbar show fairly low Fe^{3+}/Fe^{2} ratios corresponding to pO_2 values 2–3 orders of magnitude lower than pO_2(MW). Thus, even if impact (tektite) melts were formed during a strong impact event through vapor phase condensation at relatively low pressures, the oxidation state of iron in them must be rather low.

The reduced character of high-temperature impact liquids can be retained in quenched glasses produced during the development of the explosion process via the dispersion and rapid cooling of ejected material, when the system becomes open. The region of abrupt cooling of gas–liquid impact products is tentatively shown in Fig. 18 (shaded field Q). During this nonequilibrium stage, the reverse reactions of Fe^{3+} oxidation, which could have been expected under equilibrium conditions during melt cooling owing to its interaction with the gas phase, are evidently impossible. In contrast, under the conditions of a sharp increase in the volume of the explosion cloud, when it enters the low-density layers of the atmosphere, and separation of the gas–liquid mixture, hot melts can experience some additional reduction at the expense of partial evaporation. This was observed in model experiments on the evaporation of iron-bearing melts in vacuum. In addition, the phases produced during the sharp cooling and condensation of a vapor can probably be strongly nonequilibrium with respect to the redox state. Possible examples include

metallic iron and iron oxide phases (wüstite, magnetite, and hematite). It is conceivable that the same process is reflected by the occurrence of unusual domains in tektite glasses enriched in reduced silicon species, Si^0 and Si^{2+} [82], which were observed in experiments on the condensation of silicate vapors.

CONCLUSIONS

(1) The analysis of available data on the Fe^{3+}/Fe^2 ratios of tektite and impactite melts indicated that the redox state of impact melts (glasses) may be significantly different from the redox state of the precursor target rocks. The degree of iron reduction (compared with the initial state of target rocks) in various types of impact glasses increases in the following sequence: (1) impact melt rocks (tagamites), which are practically identical to the source rocks in terms of iron oxidation; (2) impact bombs; (3) tektite-like impactites (irghizites); (4) Muong Nong-type tektites; and (5) splash-form tektites, showing the maximum degree of reduction.

(2) The analysis of redox reactions in relatively simple systems containing iron in different valence states (Fe–O and SiO_2–FeO–Fe_2O_3) showed that variations in *P–T* parameters are inevitably accompanied by redox reactions and changes in the Fe^{3+}/Fe^2 ratio of the liquid phase owing to the incongruent character of melt evaporation. Reduction (or oxidation) can occur not only at increasing temperature (thermal reduction or oxidation) and $P_{tot} \cong$ const but also in response to a pressure decrease at constant *T* or under the conditions of adiabatic cooling (decompression reduction or oxidation). These processes occur both under closed and open conditions, when the vapor phase is completely or partly removed from the system. Changes in the oxidation state of materials owing to high-temperature decompression are especially important for the understanding of the redox state of impact melts produced in the course of melting and evaporation at the stage of unloading and adiabatic decompression.

(3) The direction of redox reactions with iron in evaporating melts related to variations in *P–T* parameters (oxidation with an increase in Fe^{3+}/Fe^{2+} or reduction with a decrease in Fe^{3+}/Fe^{2+}) depends on the initial oxidation state of melts. The thermal and/or decompression evaporation of relatively oxidized melts generated at the expense of crustal rocks under isothermal or near adiabatic conditions is accompanied by the reduction of ferric iron. During the evaporation, the Fe^{3+}/Fe^{2+} ratio of residual melt must tend to some stable limiting value, which depends on melt composition and *P–T* evaporation conditions. The higher the temperature, the lower the limiting value of melt Fe^{3+}/Fe^2 ratio.

(4) Based on the analysis of redox reactions in simple iron-bearing systems (Fe–O and SiO_2–FeO–Fe_2O_3) and the available data on the influence of pO_2, *T*, and P_{tot} on the Fe^{3+}/Fe^{2+} ratio of silicate melts, we proposed a model reproducing the principal features of redox state variations during the formation of impact melts. Our model suggests that the significantly lower Fe^{3+}/Fe^{2+} values of impact melts compared with the initial relatively oxidized state of target rocks could be related to the specific features of oxygen regime during the stage of adiabatic decompression after the shock compression of materials. At some stage of decompression, the vapor pressure becomes equal to the total pressure in the system, after which a further decrease in total pressure is inevitably accompanied by pO_2 decrease and, correspondingly, partial reduction of Fe^{3+} to Fe^{2+} in the melt. One of the main prerequisites for the occurrence of reduction reactions with the participation of iron and probably some other elements of variable valence is the attainment of high temperatures (>1800–2000°C) during unloading, sufficient for the complete melting and partial evaporation of the material. Even a more significant reducing effect can be observed in melts generated by the complete (or almost complete) evaporation with subsequent condensation at temperatures of >2500–3000°C. It is possible that the above-described reduction mechanism operates most efficiently in such a case, because reaction rates in a gas phase are very high, and the redox state of the condensing liquid more closely corresponds to equilibrium conditions.

(5) The effect of decompression reduction occurs under closed-system conditions and does not require selective removal of oxygen or vapor from the system. This is in full agreement with the conditions of impact processes during the early stages of unloading. The short time scales of such processes exclude any significant selective movement of components, as well as complete or partial removal of some of them from the system. Only at the last stages of the impact process, during the stage of the dramatic expansion of the explosion cloud, dispersion, and rapid cooling, the system is already not closed. Quenched glasses formed under such nonequilibrium conditions reflect the reduced state of impact melts generated mainly during previous decompression stages. It is possible that the processes of melt evaporation and the loss of oxygen together with the vapor phase in a low-density atmosphere at rather low pressures contributed to the reduction of Fe^{3+} during this final stage. Quenched glasses formed by the rapid cooling of late-stage melt–vapor mixtures could evidently capture and retain microinclusions of the products of nonequilibrium vapor condensation containing iron compounds of various valence states, such as metallic iron and its oxides (wüstite, magnetite, and hematite).

(6) In summary, the presented data allow us to conclude that major impact events result in the formation of a series of impact melts, whose temperature is the main factor controlling their redox state. The most reduced impactites are tektites ($Fe^{3+}/\Sigma Fe \le 0.1$), which were evidently formed at the highest temperatures. The origin of some types of microtektites and tektites (e.g.,

moldavites) is assigned to the condensation of decompression-produced vapor phase during its rapid cooling [6]. On the other hand, some tektites show Fe^{3+}/Fe^{2+} variations, which are especially common in Muong Nong-type tektites with a layered structure and up to tens of centimeters in size. Variations in the iron oxidation state were observed within a single sample of Muong Nong-type tektites [20]. These observations provide compelling evidence for the heterogeneity of the medium of tektite formation: gradients in P-T-pO_2 parameters and coexistence of the vapor and liquid phases. Impact bombs and tektite-like impactites (irghizites), which are found within or near impact craters, are much more oxidized ($Fe^{3+}/\Sigma Fe \cong 0.2–0.3$) than tektites. The temperatures of their parental melts were probably much lower than the temperatures of formation of typical tektites. The degree of iron oxidation in these melts was much closer to that of the initial target rocks compared with tektites. Finally, impact melts of the tagamite type were probably generated at lowest temperature, and they do not show any significant decrease in Fe^{3+}/Fe^{2+} compared with the target rocks.

ACKNOWLEDGMENTS

The authors thank O.I. Yakovlev, S.I. Shornikov, and V.I. Fel'dman for the stimulating discussion of problems addressed in this paper and for constructive criticism. This study was financially supported by the Russian Foundation for Basic Research, project no. 02-05-64735, and the Department of Earth Sciences of the Russian Academy of Sciences, project no. 10–7 of 2005.

REFERENCES

1. A. T. Basilevsky, B. A. Ivanov, K. P. Florenskii, et al., *Impact Crater on the Moon and Planets* (Nauka, Moscow, 1983) [in Russian].
2. H. J. Melosh, *Impact Cratering: A Geologic Process* (Clarendon Press, New York, 1989; Mir, Moscow, 1994).
3. V. I. Fel'dman, *Petrology of Impactites* (Mosk. Gos. Univ., Moscow, 1990) [in Russian].
4. O. I. Yakovlev, Yu. P. Dikov, and M. V. Gerasimov, "Differentiation Caused by Impact-Induced Vaporization during the Earth's Accretion," Geokhimiya, No. 10, 1027–1045 (2000) [Geochem. Int. **38**, 937–954 (2000)].
5. C. Koeberl, "Geochemistry of Tektites and Impact Glasses," Annu. Rev. Earth Planet. Sci **14**, 323–350 (1986).
6. W. V. Engelhardt, E. Luft, J. Arndt, et al., "Origin of Moldavites," Geochim. Cosmochim. Acta **51**, 1425–1443 (1987).
7. G. Heinen, *Tektites—Witnesses of Cosmic Catostrophes* (Imprimerie, Luxembourg, 1998).
8. R. F. Fudali, M. D. Dyar, D. L. Griscom, and H. D. Schreiber, "The Oxidation State of Iron in Tektite Glass," Geochim. Cosmochim. Acta **51**, 2749–2756 (1987).
9. O. I. Yakovlev, Yu. P. Dikov, and M. V. Gerasimov, "Problems of Oxidation and Reduction in the Impact Process," Geokhimiya, No. 12, 1359–1370 (1992).
10. A. A. Kadik, O. A. Lukanin, E. V. Zharkova, and V. I. Fel'dman, "Oxygen and Hydrogen (Water) Regime during Tektite Formation," Geokhimiya, No. 9, 950–967 (2003) [Geochem. Int. **41**, 865–880 (2003)].
11. O. A. Lukanin and A. A. Kadik, "Possible Reasons of Low Fe^{3+}/Fe^{2+} Ratios in Tektites in Comparison with That of Initial Target Matter Involved in the Impact Process," in *Vernadsky Institute–Brown University Microsymposium 38* (Moscow, 2003).
12. O. A. Lukanin and A. A. Kadik, "Ferric Iron Reduction during Tektites Formation: Possible Influence of the Impact Processes on the Redox Conditions of Early Earth," in *Abstracts of 32nd International Geological Congress, Florence, Italy, 2004* (Florence, 2004).
13. J. A. O'Keef, *Tektites and Their Origin* (Elsevier, Amsterdam, Oxford, and New York, 1976).
14. H. D. Schreiber, L. M. Minnix, and G. B. Balazs, "The Redox State of Iron in Tektites," J. Non-Cryst. Solids **67**, 349–359 (1984).
15. E. Izokh, I. Kashkarov, and N. Korotkova, *Age and Chemical Composition of the Zhamanshine Crater Impactites and Tektites and Comparison with Australasian Tektites*, (UIGGM, Novosibirsk, 1993).
16. A. N. Thorpe, F. E. Senftle, and F. Cuttitta, "Magnetic and Chemical Investigations of Iron in Tektites," Nature **197**, 836–840 (1963).
17. C. C. Schnetzler and W. H. Pinson, Jr., "The Chemical Composition of Tektites," in *Tektites*, Ed. by J. A. O`Keefe (Univ. Chicago, Chicago, 1963) pp. 95–129.
18. C. C. Schnetzler and W. H. Pinson, "A Report on Some Recent Major Element Analyses of Tektites," Geochim. Cosmochim. Acta **28**, 793–806 (1964).
19. R. A. Dunlap, D. A. Ealman, and G. R. MacKay, "A Mössbauer Effect Investigation of Correlated Hyperfine Parameters in Natural Glasses (Tektites)," J. Non-Cryst. Solids **223**, 141–146 (1998).
20. B. P. Glass, C. Koeberl, J. D. Blum, et al., "A Muong-Nong-Type Georgia Tektite," Geochim. Cosmochim. Acta **59**, 4071–4082 (1995).
21. S. R. Taylor, "The Chemical Composition of Australites," Geochim. Cosmochim. Acta **28**, 685–722 (1964).
22. S. R. Taylor and M. Sachs, "Geochemical Evidence for the Origin of Australites," Geochim. Cosmochim. Acta **28**, 235–264 (1964).
23. F. Cuttitta, E. C. T. Chao, M. K. Carron, et al., "Some Physical Properties and the Chemical Composition of Australasian Tektites," U.S.G.S. Astrogeol. Studies Annu. Prog. Rept. Part C, 1–52 (1964).
24. N. N. Karataeva, F. V. Polosin, and T. V. Malysheva, "Valent and Coordination State of Iron in Tektites and Impactites," Geokhimiya, No. 6, 899–903 (1985).
25. C. Koeberl, F. Kluger, and W. Kiesl, "Geochemistry of Muong Nong Tektites V: Unusual Ferric/Ferrous Ratios," Meteoritics **19**, 253–254 (1984).
26. S. Rossano, E. Balan, G. Morin, et al., "^{57}Fe Mössbauer Spectroscopy of Tektites," Phys. Chem. Minerals **26**, 530–538 (1999).

27. A. A. Kotel'nikova, V. S. Rusakov, O. A. Lukanin, and A. A. Kadik, "Mössbauer Studies of Iron State in Tektites," in *Abstracts of Annual Seminar on Experimental Mineralogy, Petrology, and Geochemistry, Moscow, Russia, 2003* (GEOKhI, Moscow, 2003), pp. 31–32 [in Russian].
28. J. A. Philpotts and W. H. Pinson, "New Data on the Chemical Composition and Origin of Moldavites," Geochim. Cosmochim. Acta **30**, 253–66 (1966).
29. F. Cuttitta, M. K. Carron, and C. Annell, "New Data on Selected Ivory Coast Tektites," Geochim. Cosmochim. Acta **36**, 1297–1309 (1972).
30. P. V. Florenskii, "Zhamanshin Meteorite Crater, Northern Priaral'e, and Its Tektites and Impactites," Izv. Akad. Nauk SSSR, Ser. Geol. **10**, 73–86 (1975).
31. L. S. Walter and A. S. Doan, "Determination of the PO_2–T Equilibrium of Indoshinite Tektite (Abstr.) NASA Astrophysics Data System (ADS)," Meteoritic. Soc. **4**, 295–296 (1969).
32. R. Brett and M. Sato, "Intrinsic Oxygen Fugacity Measurements of 7 Chondrites and Pallasite, and Redox State of Meteorite Parent Bodies," in *Proceedings of 14th Lunar and Planetary Science Conference, Houston, USA, 1983* (Lunar and Planetary Inst., Houston, 1983), pp. 69–70.
33. *Petrography*, Ed. by A. A. Marakushev (Mosk. Gos. Univ., Moscow, 1981), Vol. 2 [in Russian].
34. W. T. Huang, *Petrology* (McGraw-Hill, New York, 1962; Mir, Moscow, 1965).
35. B. D. Dressler and W. U. Reimold, "Terrestrial Impact Rocks and Glasses," Earth Sci. Rev. **56**, 205–284 (2001).
36. W. V. Engelhardt, "Shock Produced Rock Glasses from the Ries Crater," Contrib. Mineral. Petrol. **36**, 265–292 (1972).
37. R. A. F. Grieve, G. Reny, E. P. Gurov, and V. A. Ryabenko, "The Melt Rocks of the Boltysh Impact Crater, Ukraine, USSR," Contrib. Mineral. Petrol. **96**, 56–62 (1987).
38. R. Rost, *Vltaviny a Tektity* (Academia, Praha, 1972).
39. W. v. Engelhardt, "Chemical Composition of Ries Glass Bombs," Geochim. Cosmochim. Acta **31**, 1677–1689 (1967).
40. W. v. Engelhardt and G. Graup, "Suevite of the Ries Crater," Geol. Rundsch. **73**, 447–481 (1984).
41. M. V. Volovetskii, V. S. Rusakov, and O. A. Lukanin, "Mössbauer Studies of Valent and Structural State of Iron Atoms in Tektites, Impactites, and Obsidianes," in *Proceedings of International Conference on Spectroscopy, X-Ray Diffractometry, and Crystal Chemistry of Minerals, Kazan, Russia, 2005* (Kazan, 2005), pp. 48–50 [in Russian].
42. G. Giuli, G. Pratesi, C. Copriani, and E. Paris, "Iron Local Structure in Tektites and Impact Glasses by Extended X-Ray Absorption Fine Structure and High Resolution X-Ray Absorption Near-Edge Structure Spectroscopy," Geochim. Cosmochim. Acta **66**, 4347–4353 (2002).
43. A. I. Raikhlin, A. D. Kirikov, and V. S. Kozlov, "Fe^{3+} in Impact Glasses and Tektites," Dokl. Akad. Nauk SSSR **287**, 422–424 (1986).
44. R. M. Mineeva, L. V. Bershov, A. S. Marfunin, et al., "Structural Forms of Iron and Manganese in Tektites and Impactites Based on EPR Data," Mineral. Zh. **6** (3), 30–35 (1984).
45. *Explosive Ring Structures of Shields and Platforms* (Moscow, 1985) [in Russian].
46. L. J. Spencer, "Meteoric Iron and Silica-Glass from the Meteorite Craters of Henbury (Central Australia) and Wabar (Arabia)," Mineral. Mag. **23**, 387–404 (1933).
47. A. El Goresy, "Die Erzminerale in den Ries- und Bosumtwi-Krater-Glasern und ihre genetische Bedeutung," Geochim. Cosmochim. Acta **28**, 1881–1884 (1964).
48. E. C. T. Chao, E. J. Dwornik, and C. W. Merrill, "Nickel–Iron Spherules from the Aouelloul Glass of Mauritania, Africa," Science **154**, 759–765 (1966).
49. S. Fregerslev and H. Carstens, "FeNi Metal in Impact Melt Rocks of Lake Lappajarvi, Finland," Contrib. Mineral. Petrol. **55**, 255–263 (1976).
50. S. A. Vishnevsky and J. Raitala, "Native Iron, Wustite and Magnetite in Impactites of Janisjarvi and Grandos Craters (the Baltic shield)," in *Proceedings of 66th Annual Meteoritical Society Meeting* (2003), No. 5072.
51. E. I. Sandimirova, S. F. Glavatskikh, and S. N. Rychagov, "Magnetic Spherules from Volcanogenic Rocks of the Kurile Islands and Southern Kamchatka," Vestn. KRAUNTs Nauki o Zemle, No. 1, 135–139 (2003).
52. E. C. T. Chao, I. Adler, E. J. Dwornik, and J. Littler, "Metallic Spherules in Tektites from Isobela, Philippine Islands," Science **135**, 97–98 (1962).
53. E. C. T. Chao, E. J. Dwornik, and J. Littler, "New Data on the Nickel–Iron Spherules from Southeast Asian Tektites and Their Implications," Geochim. Cosmochim. Acta **28**, 971–980 (1964).
54. R. Brett, "Metallic Spherules in Impactite and Tektite Glasses," Am. Mineral. **52**, 721–733 (1967).
55. J. B. Barrat, B. M. Jahn, J. Amosse, et al., "Geochemistry and Origin of Libyan Desert Glasses," Geochim. Cosmochim. Acta **61**, 1953–1959 (1997).
56. G. G. Vorob'ev, "Studies of Tektite Composition. I. Indochinite," Meteoritika **17**, 64–72 (1959).
57. H. Fechtig and B. Kleinman, "Metallische Einschlusse in Tektiten," Fortschritt. Mineral. **44**, 144–145 (1967).
58. A. N. Thorpe and F. E. Senftle, "Submicroscopic Spherules and Color of Tektites," Geochim. Cosmochim. Acta **28**, 981–992 (1964).
59. T. Werner and G. J. Borradaile, "Homogeneous Magnetic Susceptibilities of Tektites: Implications for Extreme Homogenization of Source Material," Phys. Earth Planet. Inter. **108**, 235–243 (1998).
60. L. S. Darken and R. W. Gurry, "The System Iron–Oxygen. I. The Wüstite Field and Related Equilibria," Am. Chem. Soc. J. **67**, 1398–1412 (1945).
61. L. S. Darken and R. W. Gurry, *Physical Chemistry of Metals* (McGraw-Hill, New York, 1953; Metallurgizdat, Moscow, 1960).
62. A. Muan and E. F. Osborn, *Phase Equilibria among Oxides in Steelmaking*, (Addison-Wielley, Massachusets, 1965).
63. I. S. Kulikov, *Thermal Dissociation of Compounds* (Metallurgiya, Moscow, 1969) [in Russian].

64. I. S. Kulikov, *Thermodynamics of Oxides. A Handbook* (Moscow, 1986) [in Russian].
65. N. A. Toropov, V. V. Bazarkovskii, N. A. Bondar', and Yu. P. Udalov, *Phase Diagrams for Silicate Systems. A Reference Book. Issue 2. Metal–Oxygen Compounds of Silicate Systems* (Nauka, Leningrad, 1970) [in Russian].
66. A. Sheffler and H. J. Melosh, "Why Moldavites Are Reduced," in *Lunar and Planetary Science XXXVI* (Houston, 2005), No. 1468.
67. L. S. Walter and M. K. Carron, "Vapor Pressure and Vapor Fractionation of Silicate Melts of Tektite Composition," Geochim. Cosmochim. Acta **28**, 937–951 (1964).
68. P. I. Ozhegov, V. A. Glotov, A. V. Merzlyakov, et al., "Change in the Valence State of Iron in Basalts during Evaporation in Vacuum," Geokhimiya, No. 8, 1229–1232 (1973).
69. J. Konta and L. Mraz, "Volatility of Oxides from Silicate Melt and the Origin of Moldavites," Mineral. Mag. **40**, 70–78 (1975).
70. A. Hashimoto, "Evaporation Metamorphism in the Early Solar Nebula—Evaporation Experiments on the Melt FeO–MgO–SiO_2–CaO–Al_2O_3 and Chemical Fractionations of Primitive Materials," Geochem. J. **17**, 111–145 (1983).
71. O. M. Markova, O. I. Yakovlev, G. A. Semenov, and A. N. Belov, "Some General Results of Experiments on the Evaporation of Natural Melts in a Knudsen Cell," Geokhimiya, No. 11, 1559–1568 (1986).
72. J. Wang, A. M. Davis, R. N. Clayton, et al., "Chemical and Isotopic Fractionation during the Evaporation of the FeO–MgO–SiO_2–CaO–Al_2O_3–TiO_2 Rare Element Melt System," Geochim. Cosmochim. Acta **65**, 479–494 (2001).
73. O. I. Yakovlev, Yu. P. Dikov, M. V. Gerasimov, et al., "Experimental Investigation of Factors Controlling the Composition of Glasses from the Lunar Regolith," Geokhimiya, No. 5, 467–481 (2003) [Geochem. Int. **41**, 417–430 (2003)].
74. M. V. Gerasimov, Yu. P. Dikov, and O. I. Yakovlev, "Reduction of W, Mn, and Fe during High Temperature Vaporization," in *Lunar and Planetary Science XXXV* (Houston, 2004), No. 1491.
75. S. I. Shornikov, "Thermodynamic Regularities of Evaporation Processes of CMAS Compounds," in *Lunar and Planetary Science XXXV* (Houston, 2004), No. 1058.
76. R. O. Sack, I. S. E. Carmichael, M. Rivers, and M. S. Ghiorso, "Ferric–Ferrous Equilibria in Natural Silicate Liquids at 1 Bar," Contrib. Mineral. Petrol. **75**, 369–378 (1980).
77. A. Kilinc, I. S. E. Carmichael, and M. Rivers, "The Ferric–Ferrous Ratio of Natural Silicate Liquids Equilibrated in Air," Contrib. Mineral. Petrol. **83**, 136–140 (1983).
78. G. S. Nikolaev, A. A. Borisov, and A. A. Ariskin, "Calculation of the Ferric–Ferrous Ratio in Magmatic Melts: Testing and Additional Calibration of Empirical Equations for Various Magmatic Series," Geokhimiya, No. 8, 713–722 (1996) [Geochem. Int. **34**, 641–649 (1996)].
79. V. Kress and I. S. E. Carmichael, "The Compressibility of Silicate Liquids Containing Fe_2O_3 and the Effect of Composition, Temperature, Oxygen Fugacity and Pressure on Their Redox States," Contrib. Mineral. Petrol. **108**, 82–92 (1991).
80. O. A. Lukanin, V. S. Rusakov, A. A. Kotel'nikova, and A. A. Kadik, "Valence and Structural State of Iron in Basaltic Melts at Pressures up to 5 kbar," Petrologiya **10**, 339–363 (2002) [Petrology **10**, 299–320 (2002)].
81. H. Ramberg, "Temperature Changes Associated with Adiabatic Decompression in Geological Processes," Nature, **234**, 539–540 (1971).
82. N. A. Ashikhmina, O. A. Bogatikov, Yu. P. Dikov, et al., *Natural Glasses—Indicators of Geological Processes* (Nauka, Moscow, 1987) [in Russian].